Bioorganic Chemistry 112 (2021) 104985

Contents lists available at ScienceDirect

Bioorganic Chemistry

journal homepage: www.elsevier.com/locate/bioorg

Insight on a new indolinone derivative as an orally bioavailable lead compound against renal cell carcinoma

Marwa A. Fouad [a,*], Mayssoune Y. Zaki [b], Raghda A. Lotfy [b], Walaa R. Mahmoud [a]

[a] Pharmaceutical Chemistry Department, Faculty of Pharmacy, Cairo University, El-Kasr El-Eini Street, P.O. Box 11562 Cairo, Egypt
[b] Applied Organic Chemistry Department, National Organization for Drug Control and Research (NODCAR), Giza, Egypt

ARTICLE INFO

Keywords:
Indolinone
Sunitinib
Renal cell carcinoma
PDGFR
CDK
Cell cycle arrest
Oral bioavailability

ABSTRACT

A series of novel 3-indolinone-thiazolidinones and oxazolidinones **4a-k** was synthesized *via* molecular hybridization approach and sequentially evaluated to explore its cytotoxic activity. The cytotoxicity screening pointed toward the *N*-cyclohexyl thiazolidinone derivative **4f** that revealed promising renal cytotoxicity against CAKI-1 and UO-31 renal cancer cell lines with IC_{50} values 4.74 and 3.99 μM, respectively, which were comparable to those of sunitinib along with good safety threshold against normal renal cells. Further emphasis on compound **4f** renal cytotoxicity was achieved *via* different enzyme assays and CAKI-1 and UO-31 cell cycle analysis. The results were supported by *in silico* studies to explore its physicochemical, pharmacokinetic and drug-likeness properties. Finally, compound **4f** was subjected to an *in vivo* pharmacokinetic study through two different routes of administration showing excellent oral bioavailability. This research represents compound **4f** as a promising candidate against renal cell carcinoma.

1. Introduction

Cancer describes a condition where cellular changes cause the uncontrolled growth and division of cells with more than 1.9 million expected new cases in 2021 [1]. Kidney cancer represents the third tumor of the urinary tract most frequently diagnosed in adults [2]. Renal cell carcinoma (RCC) is the most common type of kidney cancer. It is highly aggressive in nature and is the most lethal type among the urologic malignancies with estimated 13.780 deaths in 2021 [1]. The pathogenesis of RCC involves alteration in genes associated with angiogenesis and consequently this type of tumor is usually rich in vasculature [3,4]. Accordingly, current RCC treatments rely on tyrosine kinase inhibitors that target the VEGF signaling axis associated with angiogenesis process and consequently, inhibitors of VEFGR (vascular endothelial growth factor receptor) and PDGFR (platelet-derived growth factor receptor) became the glowing hope as first line treatment of RCC [5].

In 2006, the indolinone-based drug sunitinib **I** was the first anti-angiogenic drug approved by the US FDA for the treatment of imatinib-resistant advanced RCC [6,7]. Sunitinib is considered as multi inhibitor of tyrosine kinases including VEGFR, PDGFR and c-KIT [8] and hence, it is considered as the first-line standard treatment for RCC displacing the traditional immunotherapy technique [9–11]. Unfortunately, several researches reported sunitinib therapy resistance which necessitates further emphasis on other potential candidates for treating RCC [12–20].

Accordingly, it deemed of interest to focus on other anti-VEGF 3-substituted indolinone drugs as semaxanib **II** [21,22], nintedanib **III** [23] and orantinib **IV** [24] with pronounced inhibitory activity. In addition to the above mentioned facts, 1*H*-indole-2,3-dione (isatin) derivatives are valuable precursors with variable biological activities [25,26] and pronounced anticancer activity with different mechanisms [27–33] against variable types of tumors as exemplified by compounds **V-IX** with potent antitumor activity such as renal carcinoma [34], metastatic advanced solid tumors [35], liver carcinoma [36] and colon carcinoma [37,38]. These mentioned data pointed toward this class of compounds as promising antitumor scaffolds (Fig. 1). In the same vein, hybridization of indolinone moiety with other five or six membered heterocycles would augment the expected antitumor activity [28,38–40].

In the light of the aforementioned findings, it seemed beneficial to incorporate the indolinone ring together with suitable 5-membered heterocycles. Accordingly, the aim of this work was to design and synthesize different indolinone-*N*-substituted thiazolidinone/oxazolidinone hybrids with promising anticancer activity and efficient

* Corresponding author.
E-mail address: marwa.fouad@pharma.cu.edu.eg (M.A. Fouad).

https://doi.org/10.1016/j.bioorg.2021.104985
Received 18 January 2021; Received in revised form 5 May 2021; Accepted 10 May 2021
Available online 12 May 2021

pharmacokinetic profile that would be better or comparable to sunitinib that is currently developing resistance against RCC.

2. Results and discussion

2.1. Chemistry

The indolinone-based compounds **4a-k** were synthesized according to Scheme 1 where firstly, different isocyanates/thiocyanates were reacted with hydrazine hydrate to form semi/thiosemicarbazide derivatives **1a-k** that were found to be in accordance with their reported data [41–46]. The formed intermediates **1a-k** were then reacted with the key compound isatin **2** in absolute ethanol in presence of few drops of glacial acetic acid [47] to obtain different hydrazine carboxamide/thioamide intermediates **3a-k** [47–52]. Finally, cyclization of the open structures **3a-k** was achieved *via* the reaction with chloroacetic acid in glacial acetic acid and fused sodium acetate to get the final compounds **4a-k**. Interestingly, the structure of the 5-membered ring obtained varied according to the reaction conditions, where conducting the reaction in glacial acetic acid afforded the thiazolidinone **4a-g** and oxazolidinone **4h-k** derivatives [53,54] while performing the reaction under basic conditions such as pyridine [55] or potassium hydroxide [56] afforded the thioxoimidazolidinone/imidazolidinedione derivatives.

The IR spectra of compounds **4a-k** revealed additional C=O stretching band along with that of indolinone in the range of 1666–1747 cm^{-1}. ^{1}H NMR spectra of all the final compounds **4a-k** displayed a singlet signal corresponding to the two protons of CH_2 group of the thiazolidinone/oxazolidinone ring at 4.0–4.37 ppm confirming the cyclization process, in addition to the appearance of aliphatic signals matching the expected pattern of CH_3, C_2H_5, butyl, and chloroethyl groups in compounds **4b-d** and **4i**, and the characteristic pattern of the allylic protons in compound **4e**. In the same vein, multiplet signals integrated for the ten cyclohexyl protons were observed in the range of 1.25–2.40 and 1.13–3.56 ppm in compounds **4f** and **4j**, respectively. Meanwhile, an increase in the integration of the aromatic protons confirmed the additional phenyl rings in compounds **4 g** and **4 k**. ^{13}C NMR of all the compounds were in accordance with their proposed carbon skeleton confirming the cyclization step showing the signal of the CH_2 carbon at 30.2–38.4 ppm and the added carbonyl carbon in the range of 169.0–174.4 ppm.

2.2. Biological evaluation:

2.2.1. Antiproliferative activity

2.2.1.1. In vitro anticancer activity as primary single high dose (10 μM) screening. Initially, all the final synthesized compounds **4a-k** were selected to be screened at a single high dose (10 μM) against a panel of sixty cancer cell lines by the NCI Developmental Therapeutic Program (www.dtp.nci.nih.gov) to evaluate their cytotoxicity at concentration 10 μM against sixty cancer cell lines, for more information see **Table S1 (Appendix A)**.

The examination of the growth inhibition results revealed that generally the thiazolidinone derivatives (**4a-g**) showed a broader spectrum than the oxazolidinone derivatives (**4 h-k**) which exhibited weak growth inhibition % (GI %). All the compounds demonstrated cytotoxic behavior activity against the ovarian and renal cell lines with compound **4f** exhibiting the broadest spectrum cytotoxic activity among all the screened compounds, with different degrees of GI % against nearly all the screened tumor cell types. This compound displayed a focused

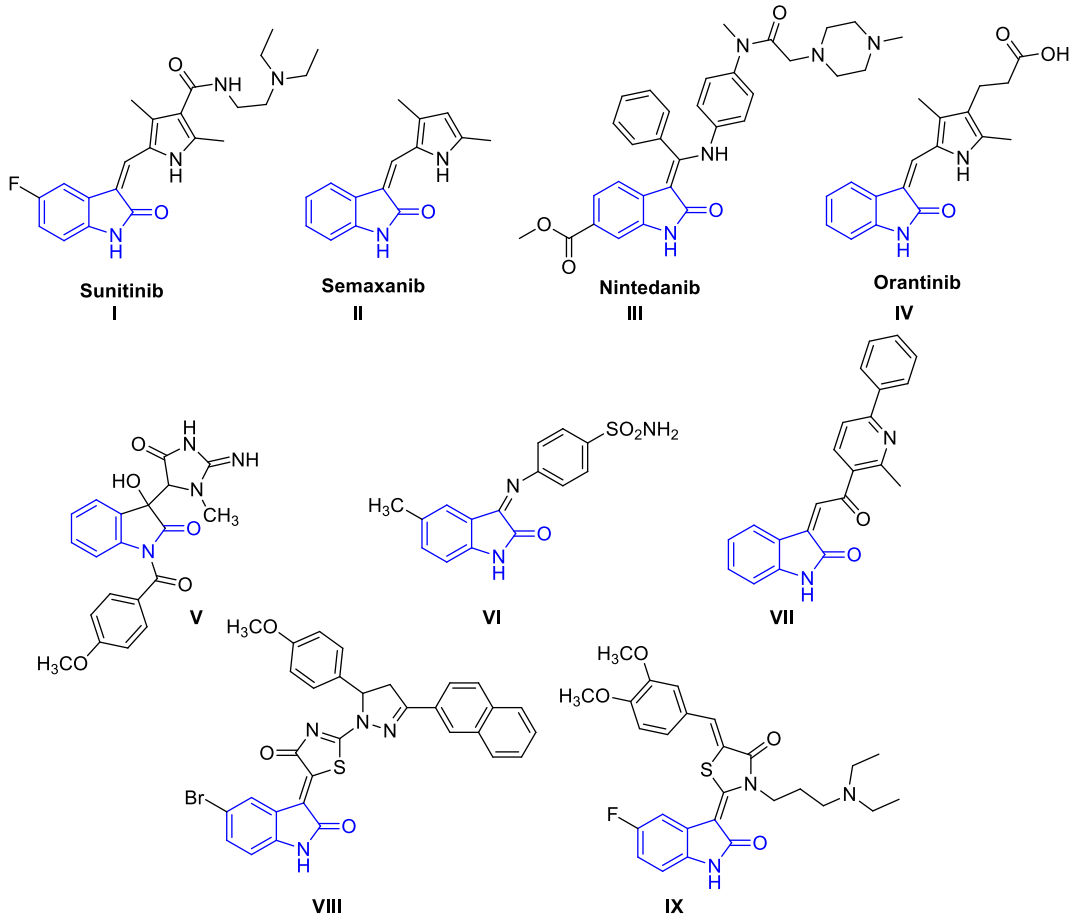

Fig. 1. Structure of indolinone-based antitumor drugs (**I-IV**) and compounds **V-IX.**

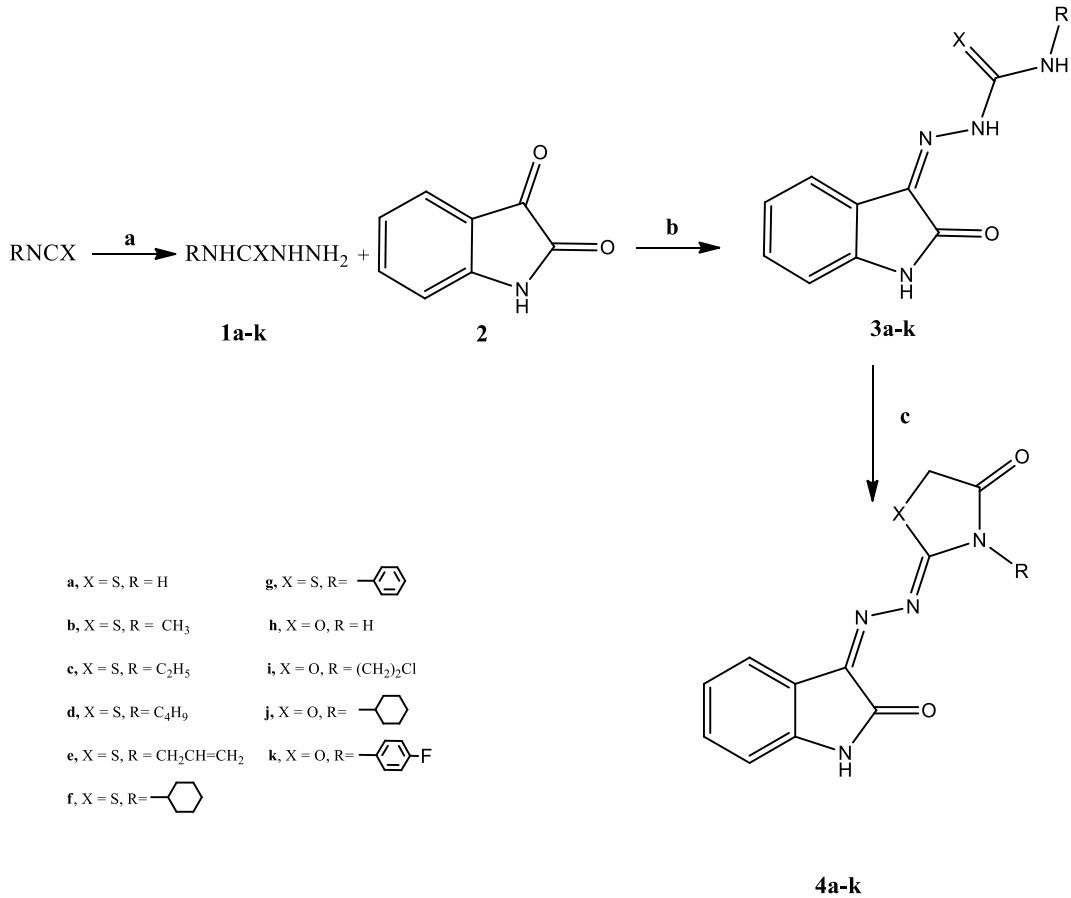

Scheme 1. Reaction conditions: (a) Hydrazine hydrate 85%, ethanol, stir, room temperature, 30 min., (b) Absolute ethanol, glacial acetic acid, reflux, 2-44 h, (c) Chloroacetic acid, glacial acetic acid, fused sodium acetate, reflux, 6-35 h.

activity against colon KM12, melanoma UACC-62 and ovarian IGROV1 and SK-OV-3 cancer cell lines with GI %= 84.9, 60, 65.9, 74.1, respectively, for more information, see **Table S1 (Appendix A)**. Moreover, compound **4f** demonstrated significant clustered cytotoxic activity against 5 renal cancer cell lines namely A498, ACHN, CAKI-1, RXF393 and UO-31 with GI % = 69.5, 59.6, 77.7, 78.4 and 61.4, respectively (For more information see **Figure S1**, See **Appendix A)**. In addition, Compounds **4d** and **4 g** showed moderate GI % against 11 and 9 cancer cell lines in the range of 30 – 56 % and 31–50%, respectively.

2.2.1.2. SAR studies. The structure–activity relationship of the synthesized final compounds was investigated for A498, ACHN, CAKI-1, RXF393 and UO-31 renal cell lines, since the inhibition effect of most of these compounds was well noticeable on the growth of these cell lines, (Table 1).

Generally, the cytotoxic activity is significantly increased by isosteric replacement of the oxygen atom in the oxazolidinone derivatives **(4 h-k)** (GI %= 5.87–11.65) with a sulfur atom in the thiazolidinone derivatives (**4a-g**) (GI %= 16.61–69.38). Comparing the derivatives substituted with an aliphatic side chain, it was observed that its elongation to four carbons as in **4d** (GI %= 23.94–47.31) afforded more enhanced activity than two carbons as in **4c** (GI %= 17.58–40.98), more than one carbon as in **4b** (GI %= 1.08–33.56). On the other side, incorporation of a double bond in the aliphatic side chain generally decreased the cytotoxic activity as shown in the thiazolidinone derivative (**4e)** (GI %= 20.21–35.30). In addition, it was noticed that alicyclic substitution

Table 1
Growth inhibition % (GI %) of compounds **4a-k** on A498, ACHN, CAKI-1, RXF393 and UO-31 renal cell lines.

Compound	X	R	A498	ACHN	CAKI-1	RXF 393	UO-31	Mean
4a	S	H	NT[a]	16.940	23.980	0	40.299	20.305
4b	S	CH_3	12.239	13.209	22.989	1.083	33.557	16.615
4c	S	C_2H_5	17.580	23.099	40.980	23.477	39.488	28.925
4d	S	C_4H_9	35.894	24.823	44.043	23.943	47.315	35.204
4e	S	$CH_2CH{=}CH_2$	22.476	20.207	35.297	28.772	32.844	27.919
4f	S		69.556	59.687	77.748	78.464	61.444	69.380
4g	S		27.854	31.254	50.388	31.801	44.632	37.186
4h	O	H	NT[a]	0	8.280	3.540	34.790	11.652
4i	O	$-CH_2CH_2Cl$	4.426	0	10.911	0	14.000	5.867
4j	O		15.073	3.988	15.758	2.948	10.296	9.613
4k	O		10.528	0	17.070	6.292	14.976	9.773

[a] NT = not tested.

exhibited a pronounced growth inhibition in the thiazolidinone derivative (**4f**) (GI %= 59.69–78.46) much more than its oxazolidinone isostere (**4j**) (% GI = 2.95–15.76). This effect is moderately decreased by ring aromatization as shown in the thiazolidinone derivative **4 g** (GI %= 27.85–50.39) when compared to the cyclohexyl substituted derivative (**4f**); an effect that is not well observed with the oxazolidinone derivative (**4 k**) (GI %= 0–17.07).

2.2.1.3. In vitro cytotoxic activity and selectivity against five renal cancer cell lines. The most active compound **4f** was further evaluated for its inhibition activity against five renal cancer lines as well as normal renal cells. The previous NCI screening at a single compound dose pointed toward the clustered renal cytotoxicity of compound **4f**. Accordingly, IC_{50} values for compound **4f** were calculated against the most vulnerable renal cancer cell lines namely A498, ACHN, CAKI-1, RXF393 and UO-31 as well as the corresponding RPTEC/TERT1 normal renal cells normal with respect to the reference drug, sunitinib, adopting an MTT colorimetric screening assay [57] to explore both its potential toxicity and selectivity. Sunitinib was the best choice here not only because of its nucleus structural similarity to compound **4f** but also for its prominent renal cytotoxicity. (Tables 2 and 3).

Clearly, the given results in Table 2 showed that the IC_{50} values of compound **4f** were all significantly different than those of sunitinib in the five renal cancer cell lines. In addition, the results revealed the superior cytotoxic activity of compound **4f** against CAKI-1 and UO-31 renal cancer cell lines compared to the rest of the investigated cell lines with IC_{50} values = 4.74 and 3.99 μM compared to sunitinib IC_{50} values = 5.51 and 2.94 μM, respectively corresponding to 0.86 and 1.35-folds relative to sunitinib. In addition, the results in Table 3 indicated that the best selectivity indices were against CAKI-1 and UO-31 renal cancer cells with 6.09 and 7.24-fold selectivity among the five-screened compounds with selectivity 1.54-fold lower than sunitinib in the normal renal cell line.

2.2.1.4. Antiangiogenic activity preliminary study. Angiogenesis is the physiological process of the growth of new blood vessels from preexisting ones under normal condition [58]. Likewise, the progression and metastasis of any tumor depends on the development of new blood vessels in and around the tumor where they could supply adequate oxygen and nutrition to the tumor cells [59–62]. The strong correlation between RCC and angiogenesis is well established [62–64] where miscoding of VHL, the tumor suppressor gene, usually results in enhanced expression of certain growth factors such as vascular endothelial growth factor (VEGF) and platelet derived growth factor (PDGF) [65] and consequently promoting abundant vascularization and aberrant activation of signaling pathways leading to cell proliferation and inhibition of apoptosis [66]. It's worth mentioning that despite the fact that activation of both PDGFR isomers evoke mitogenic signals but it was proved that stimulation of PDGFRα inhibits chemotaxis of fibroblasts and smooth muscle cells while PDGFRβ activation potently stimulates fibroblast chemotaxis [67,68]. Therefore, the pronounced renal cytotoxicity of compound **4f** can be rationalized by proving its significant antiangiogenic activity against PDGFRß isoform with IC_{50} value comparable to the well-known antiangiogenic reference drug sunitinib [68–71]. (Table 4)

Table 2
IC_{50} values (μM) of compound **4f** and sunitinib against five renal cancer cell lines.

Compound	A498	ACHN	CAKI-1	RXF393	UO-31
4f	8.1 ± 0.31*	17.47 ± 0.46*	4.74 ± 0.19*	23.57 ± 0.71*	3.99 ± 0.11*
Sunitinib	5.24 ± 0.18	5.42 ± 0.22	5.51 ± 0.26	10.55 ± 0.32	2.94 ± 0.10

* IC_{50} is significantly different from that of sunitinib at $P < 0.05$.

Table 3
Selectivity index of compound **4f** toward normal renal cell line against five renal cancer lines.

Compound	RPTEC/TERT1 (IC_{50}, μM)	Selectivity Index [a]				
		A498	ACHN	CAKI-1	RXF393	UO-31
4f	28.89 ± 2.22*	3.57	1.65	6.09	1.23	7.24
Sunitinib	18.78 ± 0.69	3.58	3.46	3.41	1.78	6.39

* IC_{50} is significantly different from that of sunitinib at $P < 0.05$.
[a] Selectivity index = IC_{50} on normal cells/IC_{50} on tumor cells.

Table 4
IC_{50} values (nM) of compound **4f** and sunitinib against angiogenesis promoting enzymes VEGFR2, PDGFRα and PDGFRß.

Compound	VEGFR2 IC_{50} [nM]	PDGFRα IC_{50} [nM]	PDGFRß IC_{50} [nM]
4f	452.53 ± 10.81*	280.916 ± 17.10*	45.013 ± 2.10*
Sunitinib	38 ± 3.92	69 ± 13.92	55 ± 1.61

*IC_{50} is significantly different from that of sunitinib at $P < 0.05$.

2.2.1.5. Cell cycle analysis and apoptosis study:. The promising IC_{50} values of compound **4f** against CAKI-1 and UO-31 renal cancer cell lines urged us to conduct its cell cycle analysis on both CAKI-1 and UO-31 renal cancer cell lines as well as an apoptotic study by Annexin V-based flow cytometric analysis.

2.2.1.6. Cell cycle analysis on CAKI-1 and UO-31 renal cancer cell lines. In this part, the effect of compound **4f** on different cell cycle phases of CAKI-1 and UO-31 renal cancer cell lines was investigated by treating the cells with concentration equals to its IC_{50} value (5.03 and 4.39 μM, respectively). Fig. 2 clarified that exposure of CAKI-1 and UO-31 renal cancer cells to compound **4f** resulted in significant cell cycle arrest at G2/M and pre-G1 phases with increase by 3.17 and 8.6 folds and by 9.51 and 13.86 folds, respectively. This was accompanied with concurrent reduction in the percentage of cells at G0-G1 and S phases by approximately 0.49 and 0.46 folds and at the S phase by approximately 0.71 and 0.97 folds, respectively compared to the renal cancer cell without any treatment [72,73].

2.2.1.7. Annexin-V FTIC apoptotic study. The apoptotic effect of compound **4f** was studied using Annexin-V FTIC/PI dual staining assay at its IC_{50} concentration on CAKI-1 and UO-31 renal cancer cell lines. The results revealed the apoptotic impact of compound **4f** displaying a pronounced increase in the percentage of positive apoptotic cells in (Upper Right + Lower Right) quadrants from 1.52% to 18.2% and from 1.52% to 23.97%, respectively in CAKI-1 and UO-31 renal cell lines which comprises 11.97- and 15.76- fold increase with respect to the control, respectively. In the same context, compound **4f** caused 2.94- and 6-fold increase in its necrotic ability compared to the control, (Fig. 3).

2.2.1.8. In vitro CDK inhibitory activity:. Cyclin-dependent kinases (CDKs) play crucial roles as regulators of cell progression through different phases of the cell cycle and are regulated by phosphorylation and activated by their association with cyclins [74]. Cyclin-dependent kinase 1 enzyme (CDK1) is considered as central cell cycle regulator that drives cells through G2 phase and mitosis [75,76] while the role of CDK2 enzyme in G1 to S checkpoint activation is well documented [77]. Simultaneously, the cell cycle analysis results of compound **4f** together with its renal cytotoxicity pathed the road to explore its CDK inhibitory activity in its different isoforms; CDK1/cyclin A, CDK1/cyclin B and CDK2/ cyclin A enzymes using the well-known CDK inhibitor, roscovitine as the reference drug. The IC_{50} values were calculated using nonlinear regression analysis of their inhibition curves as shown in

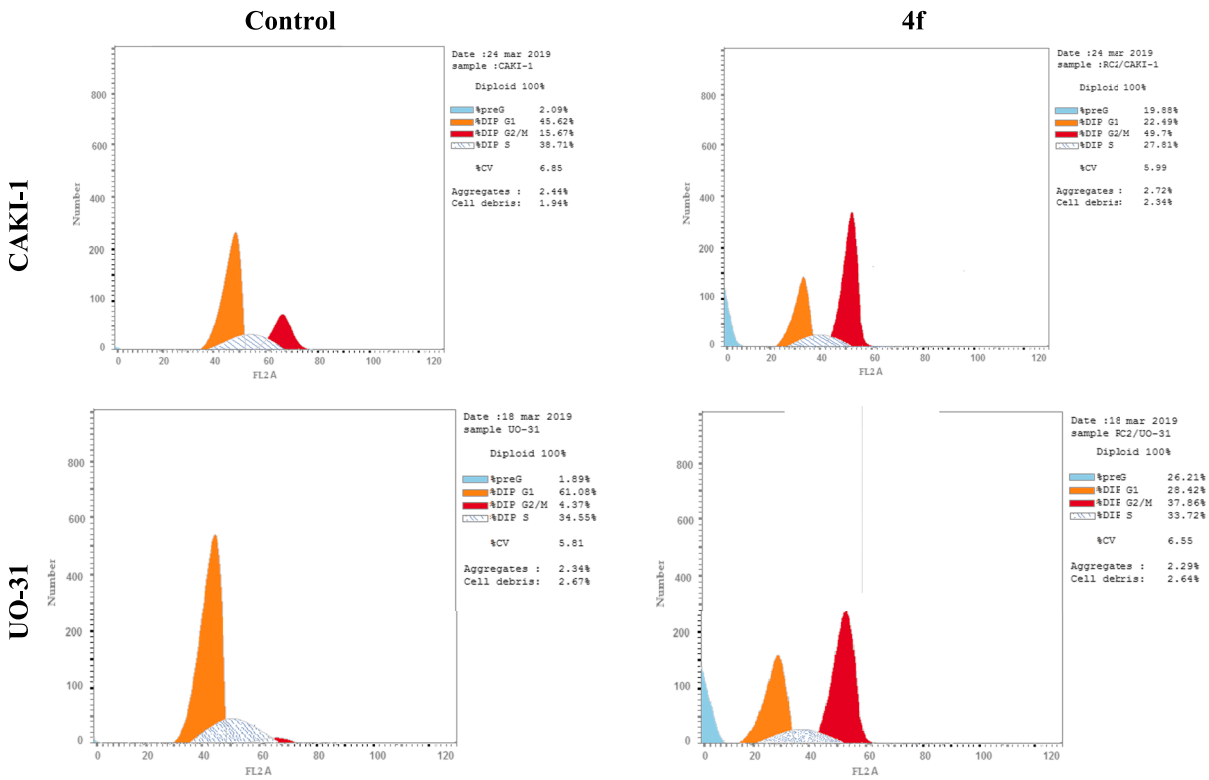

Fig. 2. Flow cytometric analysis of CAKI-1 and UO-31 renal cancer cell lines untreated and treated with compound **4f**.

Table 5. Closer look on the results located in the nM range indicates that compound **4f** exhibited 6.1, 0.19 and 1.64-fold inhibitory potency toward CDK1/cyclin A, CDK1/cyclin B and CDK2/cyclin A enzymes, respectively compared to the corresponding value of roscovitine with significant statistical difference at $P < 0.05$. These results support the previous results of the apoptotic study with the marked increase in the percentage of positive apoptotic cells and complements its previous antiangiogenic activity against PDGFRß isoform in comparison to sunitinib.

2.3. *In silico studies*

2.3.1. *Drug likeness profile*

Physicochemical properties are important aspects to consider in drug design and drug development [78]. They affect both pharmacokinetics and pharmacological properties leading ultimately to modification in the biological activity. In this context, the physicochemical properties as well as the drug-like nature profile of compound **4f** were computed using SwissADME online web tool provided by the Swiss Institute of Bioinformatics (SIB) [79]. A summary of these predictions is shown in Table 6. The compound exhibits a predicted $\log P_{o/w}$ in a range of 1.65–3.31, moderate water solubility without blood brain barrier permeability (BBB) and thus no anticipated CNS side effects. A probable high gastrointestinal absorption is predicted, as confirmed later in the *in vivo* pharmacokinetic results. In addition, it is not expected to be a substrate of the *p*-glycoprotein, so it is not disposed drug-resistance due to its efflux mechanism used by many tumor cells [80]. Another important fact that could be concluded from table 6 is that out of the five predicted CYPs, compound **4f** inhibited three isoforms namely CYP2C9, CYPIA2 and CYP2C19 while it wasn't able to inhibit two isoforms namely CYP2D6 and CYP3A4. It is worth mentioning that CYP2C9 has great impact on the metabolism of important drug families as NSAIDs [81], antihypertensives [82] and some CNS neurotransmitters as serotonin [83] while CYP2C19 inhibition could lead to alterations in the metabolism of arachidonic acid, [84] which together with the inhibition of CYP1A2 can generate problems in the metabolism of hormones [85] and cholesterol synthesis [86,87].

Finally, compound **4f** complies with the drug-likeness properties with no violation of Lipinski (Pfizer), [88] Ghose, [89] Veber (GSK), [90] Egan (Pharmacia) [91] and Muegge (Bayer) [92] filters specified by the major pharmaceutical companies. In addition, this compound exhibits high drug-likeness and bioavailability scores. One alert for Brenk problematic fragments [93] and for Pan Assay Interfering substances (PAINS) [94] were reported due to the presence of the imine fragment. Accordingly, compound **4f** is not only with promising biological efficacy but also with encouraging pharmacokinetic and physicochemical properties **(**Table 6**)**.

2.3.1.1. Molecular docking study. By searching the protein data bank (PDB), a co-crystallized PDGFRβ protein structure with an inhibitor was not available. The only available proteins were apoprotein structures for PDGFRβ transmembrane segment and in complex with PDGF without inhibitor (PDB ID 2L6W [95] and 3MJG [96], respectively). On the other hand, a co-crystallized of PDGFRα with an inhibitor was available in the protein data bank [97]. It was reported in literature that the tyrosine kinase domain of PDGFRα and the tyrosine kinase domain of PDGFRβ share strong sequence homology [98] and this was also confirmed using UniProt (https://www.uniprot.org/) [99,100] by aligning the two proteins with the code P16234 for human PDGFRα and P09619 for human PDGFRβ resulting in 43.226% identity, 485 identical positions and 323 similar positions, For more information, **(Appendix A)**. Accordingly, it was suggested to use the available co-crystallized PDGFRα as surrogate for PDGFRβ in order to highlight the possible interactions that could possibly be the reason behind the activity of compound **4f** and to validate the ability of the synthesized compound to fit in the kinase domain. Molecular docking simulations were performed to study the binding pattern of compound **4f** in the active site of PDGFRα and this pattern was compared to that of the marketed indolinone derivative, sunitinib **I**. X-

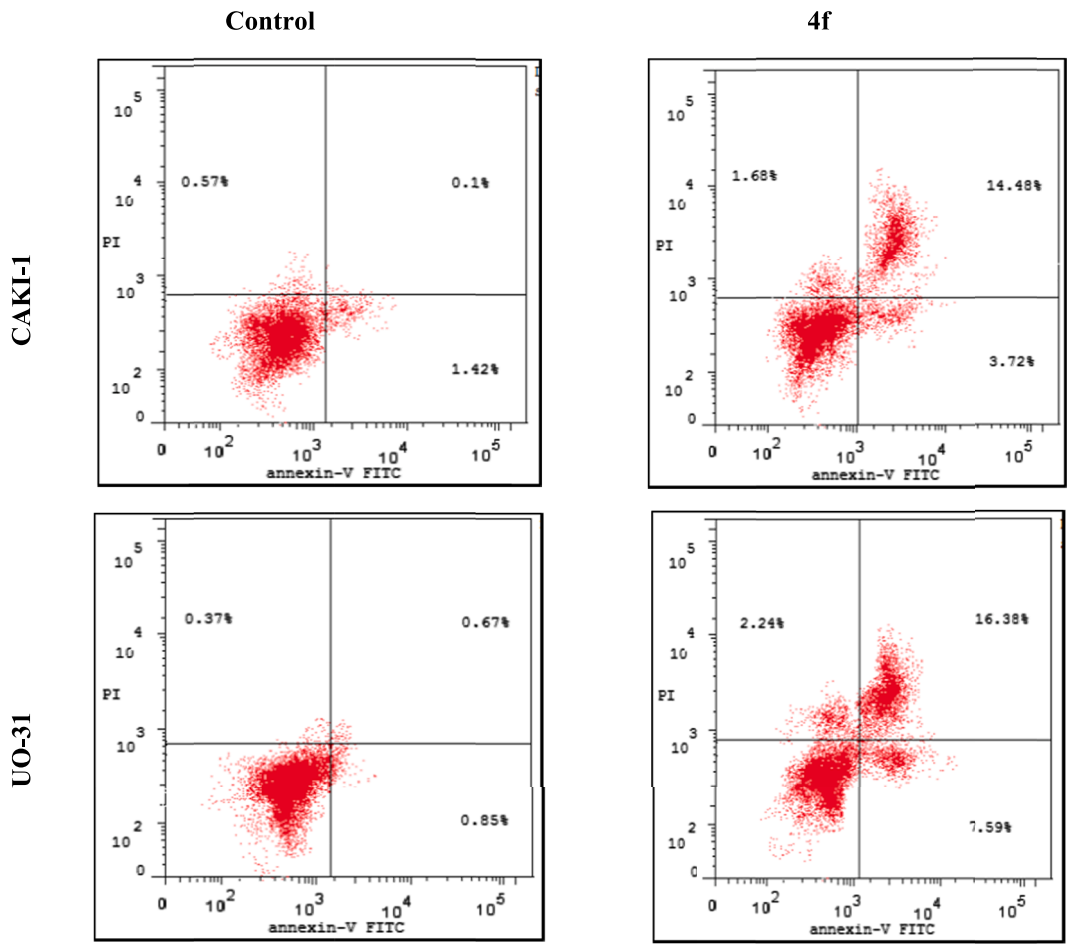

Fig. 3. Apoptotic effect of compound **4f** on CAKI-1 and UO-31 renal cancer cell lines *via* Annexin V-FTIC positive staining technique. The four quadrants are known as (LL: viable, LR: early apoptosis, UR: late apoptosis, UL: necrosis).

Table 5
IC_{50} values (nM) of compound **4f** and roscovitine against the three CDK isoforms.

Compound	CDK1/cyclin A IC_{50} [nM]	CDK1/cyclin B IC_{50} [nM]	CDK2/cyclin A IC_{50} [nM]
4f	61.014 ± 2.20*	3424.048 ± 54.09*	316.402 ± 7.35*
Roscovitine	372 ± 5.79	650 ± 16.4	520 ± 4.99

*IC_{50} is significantly different from that of roscovitine at $P < 0.05$.

ray crystal structure of PDGFRα (PDB ID: 5GRN, resolution 1.87 Å) [97] that is in complex with an inhibitor, WQ-C-159, was downloaded from the Protein Data Bank. First, the molecular docking setup was validated by carrying out re-docking of the ligand, WQ-C-159, in the vicinity of the PDGFRα active site. The applied docking protocol demonstrated to be suitable for the presented docking study by reproducing the same binding interactions of the co-crystallized ligand, as confirmed by the obtained RMSD (1.11 Å) between the native ligand and the docked one. As shown in Figs. 4 and 5, the amine and the carbonyl groups of the sunitinib indole form two hydrogen bonds with the carbonyl group and the NH group of the third hinge residue, Cys677, respectively. It also interacts hydrophobically with the residues near the ceiling of the adenine pocket including Leu599 and Val607 [101,102]. Similarly, compound **4f** forms one hydrogen bond with the NH group of Cys677 through the carbonyl group of the indolinone moiety, in addition to a hydrophobic interaction with two amino acids: Leu599 and Gly680. These similar interactions are reflected in the comparable docking scores of the new indolinone derivative, **4f** (-14.13445 kcal/mol), which displayed potent PDGFRα inhibitory activity comparable to sunitinib (-15.09492 kcal/mol). According to the sequence homology between the two isoforms of PDGFR, it can be concluded that the higher inhibition activity of compound **4f** towards PDGFRβ more than PDGFRα might be

Table 6
Molecular properties of compound **4f** predicted using SwissADME website.

Parameter	Result	Parameter	Result	Parameter	Result
Consensus Log P	2.51	**CYP2C9 inhibitor**	Yes	**Muegge #violations**	0
ESOL, Ali and Silicos-IT Class	Moderately soluble	**CYP2D6 inhibitor**	No	**Bioavailability Score**	0.55
GI absorption	High	**CYP3A4 inhibitor**	No	**PAINS #alerts**	1
BBB permeant	No	**Lipinski #violations**	0	**Brenk #alerts**	1
P-gp substrate	No	**Ghose #violations**	0	**Leadlikeness #violations**	0
CYP1A2 inhibitor	Yes	**Veber #violations**	0	**Synthetic Accessibility**	3.41
CYP2C19 inhibitor	Yes	**Egan #violations**	0		

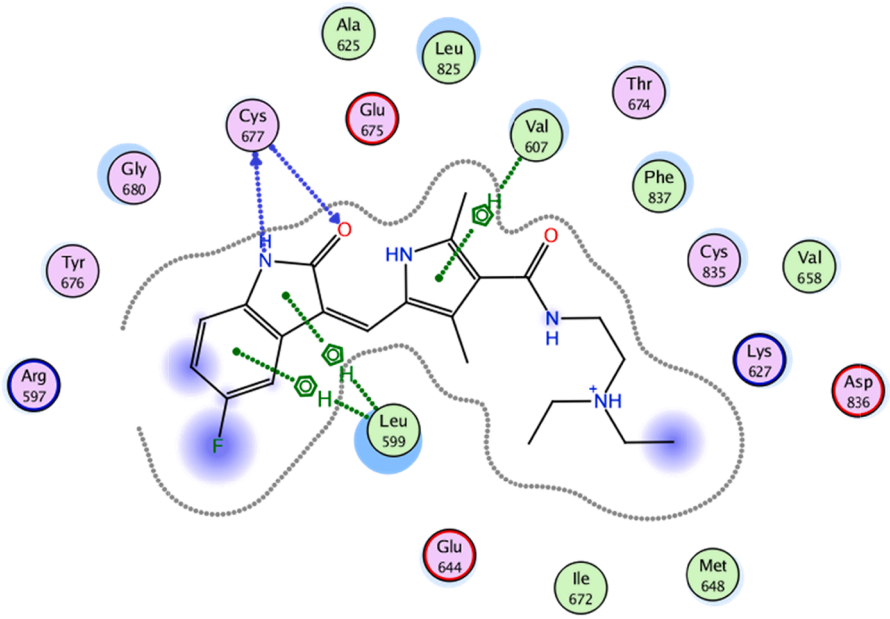

(A)

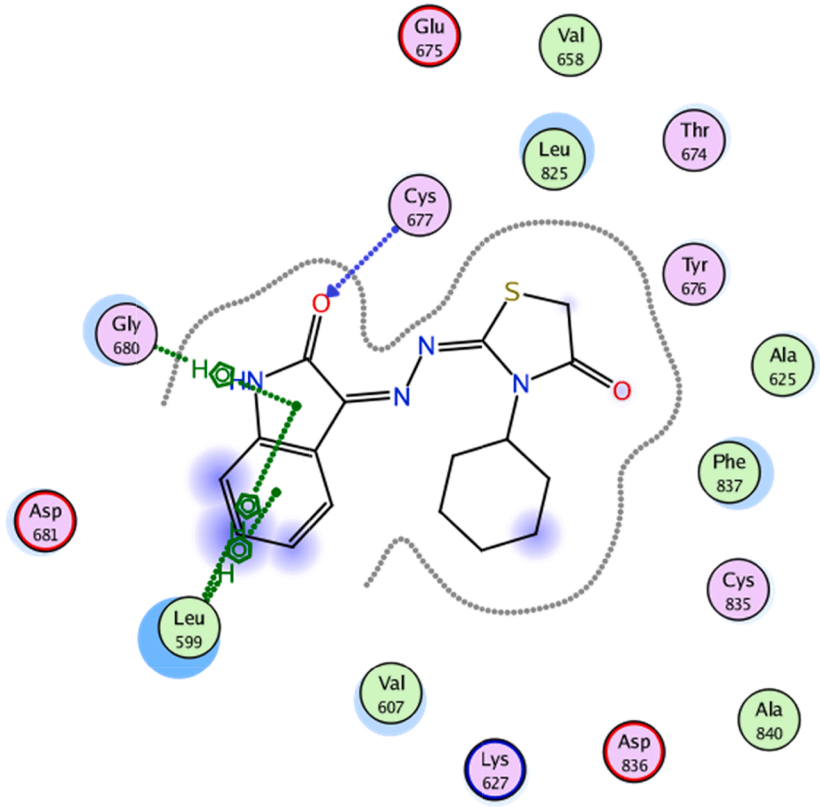

(B)

Fig. 4. 2D Diagram of the interaction of the docked (A) sunitinib and (B) **4f** in the active site of PDGFRα (PDB ID: 5GRN) using Molecular Operating Environment (MOE, 10.2008) software.

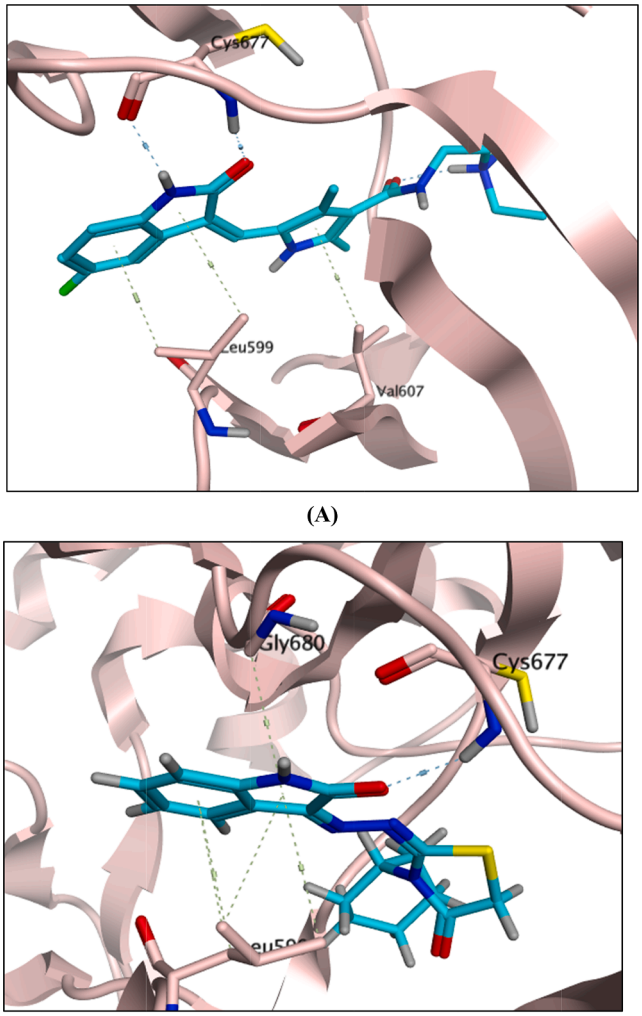

Fig. 5. 3D Representation of the interaction of the docked (A) sunitinib and (B) **4f** in the active site of PDGFRα (PDB ID: 5GRN) using Molecular Operating Environment (MOE, 10.2008) software.

justified by certain extra interactions than those shown in this molecular docking analysis with certain amino acid residues present in PDGFRβ only (Figs. 4 and 5).

2.4. *In vivo PK profile of compound **4f***

Pharmacokinetic parameters of the most potent compound **4f** was determined in male Sprague-Dawley rats, Table 7 and Fig. 6. The compound was administered intravenously (i.v.) at 5 mg/kg or orally (p.o.) at 15 mg/kg. Comparing the two routes of administration, it was found that compound **4f** demonstrated a longer half-life ($t_{1/2}$) of 18.6 h after i.v. administration than that after oral dosing (7.9 h) and this can be correlated to the difference in the two values of volume of distribution (V_d) following i.v. and oral administration (12767.7 and 4686.533 mL/kg, respectively). Comparable plasma clearance (CL) values were obtained following the two routes of administration (476.6 mL/h.kg after i.v. administration and 413.2 mL/h.kg after oral administration). Importantly, compound **4f** possessed an excellent oral bioavailability (F) of ~ 100% leading to a good oral exposure showed by AUC of 36305.6 ng.h/mL and a high maximum plasma concentration (C_{max}) of 6095.9 ng/mL after oral dosing. These results confirmed the high gastrointestinal absorption as predicted using the SwissADME web tool. The rat plasma **4f** concentration h (126.57 and 307.14 ng/mL for i.v. and p.o., respectively), was higher than the IC_{90} value required for the cytotoxic activity against CAKI-1 and UO-31 renal cancer cell line even after 24 h, as shown in Fig. 6. These important findings showed that after oral dosing in rats, compound **4f** has not only an outstanding cytotoxic activity but also good pharmacokinetic properties with excellent oral bioavailability.

Table 7
Sprague-Dawley rat pharmacokinetic profile for compound **4f** after oral and intravenous administration.

Parameter	p.o.	i.v.
Rat no.	6	6
Dose level (mg/kg)	15	5
$t_{1/2}$ (h)	7.862	18.569
T_{max} (h)	2	–
C_{max} (ng/mL)	6095.899	2281.052
AUC_{0-t} (ng.h/mL)	32821.686	7100.526
$AUC_{0-\infty}$ (ng.h/mL)	36305.602	10491.398
V_d (mL/kg)	4686.533	12767.714
CL (mL/h.kg)	413.159	476.581
F (%)	115.353%	

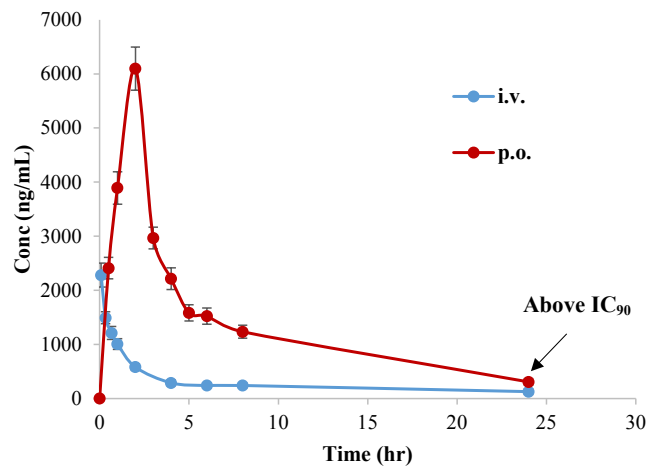

Fig. 6. Time-dependent plasma concentrations of **4f** after oral and intravenous administration to male Sprague-Dawley rats.

3. Conclusion

In conclusion, compound **4f** is a potent scaffold against renal carcinoma with excellent physiochemical, pharmacokinetic profile and interesting PDGFR/CDK inhibition activity. Accordingly, compound **4f** could be considered as a promising candidate for further preclinical and clinical studies as an anticancer agent for treatment of renal cell carcinoma.

4. Experimental

4.1. *Chemistry*

4.1.1. *General*

All solvents and reagents were commercially available and used without further purification. Compounds **1a-k** [41–46], **3a-h** [47–51], **3k** [52], **4a** [39] were prepared as reported in the literature. For more information, **(Appendix A)**.

4.1.2. *General procedure for preparation of compounds **3i** and **3j***

To a hot solution of isatin **2** (0.7 g, 5 mmol) in absolute ethanol (10 mL) containing few drops of glacial acetic acid either the semicarbazide derivative **1i** or **1j** (5 mmol) dissolved in absolute ethanol (10 mL) was

added. After then, the reaction mixture was heated to reflux for 2 h and the crystalline solid formed was collected by filtration, washed with hot ethanol then by ether to give to give both compounds in a pure form.

4.1.2.1. N-(2-Chloroethyl)-2-(2-indolinone-3-ylidene) hydrazine-1-carboxamide (3i):. Buff powder, (yield 78%), m.p. 246–247 °C; reaction time 31 h; IR (KBr, ν cm^{-1}): 3325, br. 3213 (NHs), 3097 (CH aromatic), 2939 (CH aliphatic), 1670, 1654 (2C = O); ^{1}H NMR (DMSO-d_6, 400 MHz) δ ppm: 3.80 (t, 2H, CH_2, J = 6.2), 4.90 (t, 2H, CH_2, J = 6.1), 6.65 (s, 1H, NH, D_2O exchangeable), 7.21–7.81 (m, 4H, indoline-H), 10.55 (s, 1H, NH, D_2O exchangeable), 11.35 (s, 1H, NH, D_2O exchangeable); ^{13}C NMR (DMSO-d_6) δ ppm: 41.7, 44.1, 111.3, 112.9, 126.9, 127.3, 128.7, 134.9, 139.8, 152.8, 158.9 2 (C═O); Anal. Calcd. for $C_{11}H_{11}ClN_4O_2$ (266.69): C, 49.54; H, 4.16; N, 21.01%; Found: C, 49.81; H, 4.40; N, 20.87%.

4.1.2.2. N-Cyclohexyl-2-(2-oxoindolin-3-ylidene)hydrazine-1-carboxamide (3j). Bright yellow powder, (yield 69%), m.p. 229–231 °C; reaction time 31 hr; IR (KBr, ν cm^{-1}) : 3325 (2 NH), 3032 (CH aromatic), 2927 (CH aliphatic), 1620 br. (2C = O); ^{1}H NMR (DMSO-d_6, 400 MHz) δ ppm: 1.27–1.34 (m, 5H, cyclohexyl-H), 1.55–1.72 (m, 5H, cyclohexyl-H), 1.83–1.85 (m, 1H, cyclohexyl-H), 6.90 (d, 1H, H_7-indoline, J = 7.8), 7.03 (t,1H, H_5-indoline, J = 7.6), 7.32–7.39 (m, 2H, H_6-indoline + NH, D_2O exchangeable), 8.19 (d, 1H, H4-indoline, J = 7.6), 10.30 (s, 1H, NH, D_2O exchangeable), 10.74 (s, 1H, NH, D_2O exchangeable). Anal. Calcd. for $C_{15}H_{18}N_4O_2$ (286.33): C, 63.16; H, 6.52; N, 19.34%; Found: C, 63.01; H, 6.28; N, 19.65%.

*4.1.3. General procedure for preparation of compounds **(4a-k)***

An equimolar mixture of **3a-k** (0.01 mol) and monochloroacetic acid (0.49 g, 0.01 mol) with anhydrous sodium acetate (0.82 g, 0.01 mol) in glacial acetic acid (20 mL) was refluxed for 6–35 h. Then, the reaction mixture was allowed to cool to room temperature and poured into ice water. The solid was filtered, washed with water and finally recrystallized from ethanol to give compounds **4a-k**.

4.1.3.1. 2-[(2-Oxoindolin-3-ylidene)hydrazono]thiazolidin-4-one (4a) [39]. Dark orange powder, (yield 60%), m.p. 208–210 ; reaction time 6 h; IR (KBr, ν cm^{-1}): 3417, 3174 (2 NH), 3028 (CH aromatic), 2889 (CH aliphatic), 1716 br. (2C = O); ^{1}H NMR (DMSO-d_6, 400 MHz) δ ppm: 4.01 (s, 2H, CH_2), 6.88 (d, 1H, H_7-indoline, J = 7.6), 7.04 (t, 1H, H_5-indoline, J = 7.4), 7.35 (t, 1H, H_6-indoline, J = 7.6), 8.22 (d, 1H, H_4-indoline, J = 7.8), 10.71 (s, 1H, NH, D_2O exchangeable), 11.18 (s, 1H, NH, D_2O exchangeable); ^{13}C NMR (DMSO-d_6) δ ppm: 34.0 ($\underline{C}H_2$), 110.8, 117.5, 122.4, 128.4, 132.4, 133.6, 144.9, 165.1, 173.2, 174.4 (2$\underline{C}$ = O); Anal. Calcd. for $C_{11}H_8N_4O_2S$ (260.27): C, 50.76; H, 3.10; N, 21.53%; Found: C, 51.02; H, 3.36; N, 21.31%.

4.1.3.2. 3-Methyl-2-[(2-oxoindolin-3-ylidene)hydrazono]thiazolidin-4-one (4b). Dark orange powder, (yield 64%), m.p. > 300; reaction time 9 h; IR (KBr, ν cm^{-1}): 3159 (NH), 3062 (CH aromatic), 2970 (CH aliphatic), 1732,1716 (2C = O); ^{1}H NMR (DMSO-d_6, 400 MHz) δ ppm: 3.32 (s, 3H, CH_3), 4.06 (s, 2H, CH_2), 6.88 (d, 1H, H_7-indoline, J = 7.7), 7.04 (t, 1H, H_5-indoline, J = 7.5), 7.37 (t, 1H, H_6-indoline, J = 7.6), 8.17 (d, 1H, H_4-indoline, J = 7.5), 10.75 (s, 1H, NH, D_2O exchangeable); ^{13}C NMR (DMSO-d_6) δ ppm: 30.2 ($\underline{C}H_3$), 33.0 ($\underline{C}H_2$), 110.9, 117.4, 122.6, 129.0, 133.3, 144.7, 149.2, 165.2, 172.9, 173.0 (2$\underline{C}$ = O); Anal. Calcd. for $C1_2H_{10}N_4O_2S$ (274.30): C, 52.55; H, 3.67; N, 20.43%; Found: C, 52.81; H, 3.90; N; 20.19%.

4.1.3.3. 3-Ethyl-2-[(2-oxoindolin-3-ylidene)hydrazono]thiazolidin-4-one (4c). Light orange powder, (yield 66%), m.p. > 300 °C ; reaction time 9 h; IR (KBr, ν cm^{-1}): 3429 (NH), 3082 (CH aromatic), 2970 (CH aliphatic), 1732, 1705 (2C = O); ^{1}H NMR (DMSO-d_6, 400 MHz) δ ppm: 1.27 (t, 3H, CH_3, J = 7.0), 3.90 (q, 2H, CH_2, J = 6.9), 4.07 (s, 2H, CH_2), 6.89 (d, 1H, H_7-indoline, J = 7.8), 7.04 (t, 1H, H_5-indoline, J = 7.5), 7.37 (t, 1H, H_6-indoline, J = 7.6), 8.13 (d, 1H, H_4-indoline, J = 7.5), 10.75 (s, 1H, NH, D_2O exchangeable), ^{13}C NMR (DMSO-d_6) δ ppm: 12.3 ($\underline{C}H_3$), 21.3 ($\underline{C}H_2$), 32.9 (CO$\underline{C}H_2$), 111.1, 117.1, 123.1, 128.5, 133.6, 144.0, 148.9, 165.6, 172.9, 173.1 (2$\underline{C}$ = O), Anal. Calcd. for $C_{13}H_{12}N_4O_2S$ (288.33): C, 54.16; H, 4.20; N, 19.43%; Found: C, 54.37; H, 4.38; N, 19.62%.

4.1.3.4. 3-Butyl-2-[(2-oxoindolin-3-ylidene)hydrazono]thiazolidin-4-one (4d). Brown powder, (yield 65%), m.p. 246–248 °C; reaction time 31 h; IR (KBr, ν cm^{-1}): 3182 (NH), 3089 (CH aromatic), 2958 (CH aliphatic), 1732 br. (2C = O); ^{1}H NMR (DMSO-d_6, 400 MHz) δ ppm: 0.93 (t, 3H, CH_3, J = 7.3), 1.35–1.41 (m, 2H, CH_2), 1.68–1.71 (m, 2H, CH_2), 3.86 (t, 2H, CH_2, J = 7.3), 4.08 (s, 2H, CH_2), 6.89 (d, 1H, H_7-indoline, J = 7.8), 7.01 (t, 1H, H_5-indoline, J = 7.5), 7.37 (t, 1H, H_6-indoline, J = 7.2), 8.12 (d, 1H, H_4-indoline, J = 7.5), 10.75 (s, 1H, NH, D_2O exchangeable); ^{13}C NMR (DMSO-d_6) δ ppm: 14.0 ($\underline{C}H_3$), 20.0 ($\underline{C}H_2$), 28.9 ($\underline{C}H_2$), 32.9 (CO$\underline{C}H_2$), 43.5 ($\underline{C}H_2$), 111.0, 117.4, 122.4, 128.4, 133.4, 144.7, 149.1, 165.2, 172.8, 172.9 (2$\underline{C}$ = O), Anal. Calcd. for $C_{15}H_{16}N_4O_2S$ (316.38): C, 56.95; H, 5.10; N, 17.71%; Found C, 57.11; H, 5.34; N, 17.58%.

4.1.3.5. 3-Allyl-2-[(2-oxoindolin-3-ylidene)hydrazono]thiazolidin-4-one (4e). Dark green powder, (yield 75%), m.p. 254–256 °C; reaction time 35 h; IR (KBr, ν cm^{-1}): 3429 (NH), 3086 (CH aromatic), 2981 (CH aliphatic), 1732 br. (2C = O); ^{1}H NMR (DMSO-d_6, 400 MHz) δ ppm: 4.13 (s, 2H, CH_2), 4.48 (d, 2H, CH_2, J = 4.6), 5.22 (d, 1H, =CH_2, J = 10.5), 5.26 (d, 1H, =CH_2, J = 17.4), 5.89–5.98 (m, 1H, CH), 6.88 (d, 1H, H_7-indoline, J = 7.7), 7.02 (t,1H, H_5-indoline, J = 7.6), 7.36 (t, 1H, H_6-indoline, J = 7.6), 8.11 (d, 1H, H_4-indoline, J = 7.6), 10.74 (s, 1H, NH, D_2O exchangeable); ^{13}C NMR (DMSO-d_6) δ ppm: 32.9 (N-$\underline{C}H_2$), 45.6 ($\underline{C}H_2$), 110.9, 117.3, 117.7, 122.6, 128.8, 131.4, 133.4, 144.7, 149.3, 165.2, 172.1, 172.6 (2$\underline{C}$ = O), Anal. Calcd. for $C_{14}H_{12}N_4O_2S$ (300.34): C, 55.99; H, 4.03; N, 18.66%; Found C, 56.13; H, 4.29; N, 18.53%.

4.1.3.6. 3-Cyclohexyl-2-[(2-oxoindolin-3-ylidene)hydrazono]thiazolidin-4-one (4f). Orange powder, (yield 89%), m.p. 288–290 °C; reaction time 35 h; IR (KBr, ν cm^{-1}): 3414 (NH), 3086 (CH aromatic), 2931 (CH aliphatic), 1728 br. (2C = O); ^{1}H NMR (DMSO-d_6, 400 MHz) δ ppm: 1.25–1.40 (m, 4H, cyclohexyl-H), 1.71–1.74 (m, 4H, cyclohexyl-H), 1.87–1.91 (m, 2H, cyclohexyl-H), 2.34–2.40 (m, 1H, cyclohexyl-H), 4.03 (s, 2H, CH_2), 6.91 (d, 2H, H_7-indoline, J = 7.8), 7.04 (t, 1H, H_5-indoline, J = 7.3), 7.39 (t, 1H, H_6-indoline, J = 7.9), 8.19 (d, 1H, H_4-indoline, J = 7.5), 10.77 (s, 1H, NH, D_2O exchangeable); ^{13}C NMR (DMSO-d_6) δ ppm: 25.3, 26.0, 28.05, 32.6 ($\underline{C}H_2$), 56.3, 111.3, 117.2, 122.4, 127.8, 133.5, 144.7, 148.6, 165.3, 173.1, 173.8 (2$\underline{C}$ = O), MS (m/z %): 342 (M^+, 82.35%), Anal. Calcd. for $C_{17}H_{18}N_4O_2S$ (342.42): C, 59.63; H, 5.30; N, 16.36%; Found: C, 59.85; H, 5.41; N, 16.59%.

4.1.3.7. 2-[(2-Oxoindolin-3-ylidene)hydrazono]-3-phenylthiazolidin-4-one (4g). Brownish orange powder, (yield 87%), m.p. >300 °C ; reaction time 24 h; IR (KBr, ν cm^{-1}): 3186 (NH), 3086 (CH aromatic), 2981 (aliphatic CH), 1728 br. (2C = O); ^{1}H NMR (DMSO-d_6, 400 MHz) δ ppm: 4.22 (s, 2H, CH_2), 6.65 (t, 1H, Ar-H, J = 7.8), 6.80 (d, 2H, Ar-H, J = 7.7), 7.22–7.27 (m, 3H, 2Ar-H + H_7-indoline), 7.49 (d, 1H, H_5-indoline, J = 7.2), 7.54–7.66 (m, 2H, H_{4+} H_6-indoline), 10.69 (s, 1H, NH, D_2O exchangeable); ^{13}C NMR (DMSO-d_6) δ ppm: 33.4 (CO$\underline{C}H_2$), 110.9, 117.1, 122.1, 128.5, 129.5, 129.6, 133.4, 135.4, 144.5, 149.8, 165.2, 172.4, 172.9 (2$\underline{C}$ = O), Anal. Calcd. for $C_{17}H_{12}N_4O_2S$ (336.37): C, 60.70; H, 3.60; N, 16.66%; Found: C, 60.89; H, 3.76; N, 16.90%.

4.1.3.8. 2-[(2-Oxoindolin-3-ylidene)hydrazono]oxazolidin-4-one (4h). Reddish brown powder, (yield 67%), m.p. >300; reaction time 33 h; IR (KBr, ν cm^{-1}): 3178, 3143 (2 NH), 3082 (CH aromatic), 2962 (CH aliphatic), 1693, 1666 (2C = O); ^{1}H NMR (DMSO-d_6, 400 MHz) δ ppm:

4.05 (s, 2H, CH_2), 6.84 (d, 1H, H_7-indoline, $J = 7.6$), 6.97 (t,1H, H_5-indoline, $J = 7.6$), 7.34 (t, 1H, H_6-indoline, $J = 7.4$), 9.06 (d, 1H, H_4-indoline, $J = 7.9$), 10.88 (s, 2H, 2NH, D_2O exchangeable); ^{13}C NMR (DMSO-d_6) δ ppm: 35.5 (CH_2), 110.0, 121.6, 122.1, 129.7, 133.0, 133.8, 144.5, 169.4 (2C = O), Anal. Calcd. for $C_{11}H_8N_4O_3$ (244.21): C, 54.10; H, 3.30; N, 22.94%; Found: C, 53.89; H, 3.47; N, 22.82%.

4.1.3.9. 3-(2-Chloroethyl)-2-[(2-oxoindolin-3-ylidene)hydrazono]oxazolidin-4-one (4i). White powder, (yield 60%), m.p. 225 °C; reaction time 12 h; IR (KBr, ν cm^{-1}): 3305 (NH), 3097 (CH aromatic), 2943 (CH aliphatic), 1747, 1666 (2C = O); ^1H NMR (DMSO-d_6 400 MHz) δ ppm: 3.57 (t, 2H, CH_2, $J = 6.5$), 3.98 (t, 2H, CH_2, $J = 5.8$), 4.37 (s, 2H, CH_2), 6.49–6.63 (m, 2H, H_5-indoline and H_7-indoline), 7.70–7.81 (m, 2H, H_4-indoline and H_6-indoline), 8.8 (1H, NH, D_2O exchangeable); ^{13}C NMR (DMSO-d_6) δ ppm: 38.4 (CO$\underline{C}H_2$), 44.1 ($\underline{C}H_2$), 64.1 ($\underline{C}H_2$), 118.5, 127.0, 137.3, 145.2, 158.4, 158.7, 159.0, 159.1, 167.7, 170.8 (2$\underline{C}$ = O), Anal. Calcd. for $C_{13}H_{11}ClN_4O_3$ (306.71): C, 50.91; H, 3.62; N, 18.27%, Found: C, 51.23; H, 3.86; N, 18.49%.

4.1.3.10. 3-Cyclohexyl-2-[(2-oxoindolin-3-ylidene)hydrazono]oxazolidin-4-one (4j). Bright yellow powder, (yield 94%), m.p. 226–227 °C; reaction time 9 h; IR (KBr, ν cm^{-1}): 3170 (NH), 3093 (CH aromatic), 2931 (aliphatic CH), 1716, 1693 (2C = O); ^1H NMR (DMSO-d_6, 400 MHz) δ ppm: 1.13–1.35 (m, 6H, cyclohexyl H), 1.58–1.81 (m, 4H, cyclohexyl H), 3.55–3.56 (m, 1H, cyclohexyl H), 4.07 (s, 2H, CH_2), 6.93 (d, 1H, H_7-indoline, $J = 7.7$), 7.08 (t, 1H, H_5-indoline, $J = 7.5$), 7.32 (t, 1H, H_6-indoline, $J = 7.6$), 7.63 (d, 1H, H_4-indoline, $J = 7.3$), 11.88 (s, 1H, NH, D_2O exchangeable); ^{13}C NMR (DMSO-d_6) δ ppm: 25.2, 25.5, 33.0 (CO$\underline{C}H_2$), 49.1, 111.2, 120.7, 120.8, 122.7, 130.8, 131.5, 141.7, 153.5, 163.1 (2$\underline{C}$ = O), Anal. Calcd. for $C_{17}H_{18}N_4O_3$ (326.36): C, 62.57; H, 5.56; N, 17.17%; Found: C, 62.34; H, 5.70; N, 17.43%.

4.1.3.11. 3-(4-Fluorophenyl)-2-[(2-oxoindolin-3-ylidene)hydrazono]oxazolidin-4-one (4k). Light yellow powder, (yield 77%), m.p. 263–265 °C; reaction time 6 h; IR (KBr, ν cm^{-1}): 3294 (NH), 3093 (CH aromatic), 2912 (aliphatic CH), 1670 br. (2C = O); ^1H NMR (DMSO-d_6, 400 MHz) δ ppm: 4.0 (s, 2H, CH_2), 7.07–7.11 (m, 3H, 2 Ar-H + H_7-indoline), 7.44–7.54 (m, 3H, 2 Ar-H + H_5-indoline), 7.95–8.05 (m, 1H, H_6-indoline), 8.68 (s, 1H, NH, D_2O exchangeable), 8.82–8.86 (m, 1H, H_4-indoline). ^{13}C NMR (DMSO-d_6) δ ppm: 34.3 (CO$\underline{C}H_2$), 115.4, 115.6, 115.8, 120.5, 120.6, 120.7, 120.8, 136.4, 136.43, 153.2, 156.62, 156.66, 159.0, 169.0 (2C = O), Anal. Calcd. for $C_{17}H_{11}FN_4O_3$ (338.30): C, 60.36; H, 3.28; N, 16.56%; Found: C, 60.48; H, 3.39; N, 16.80%.

4.2. Biological evaluation

4.2.1. Antiproliferative activity

4.2.1.1. In vitro anticancer activity as primary single high dose (10 μM) screening. The preliminary cytotoxicity study for the synthesized compounds **4a-k** was determined as described in the protocol of the National Cancer Institute (NCI), Bethesda, USA against a panel of 60 cell lines [103,104]. Cell lines was exposed to the compounds for 48 h using sulforhodamine B (SRB) protein assay [105] and then cell viability and growth was determined, as previously described [103,104].

4.2.1.2. MTT assay for cytotoxicity. The assay was performed at the Egyptian company for the production of vaccines, sera, and drugs VACSERA, Giza, EGYPT. Standard MTT colorimetric method was used to test the IC_{50} of compound **4f** against five renal cancer cell lines, A498, ACHN, CAKI-1, RXF393 and UO-31 and one normal renal cell line, RPTEC/TERT1, which were obtained from the American Type Culture Collection (ATCC) (Rockville, MD). Cell lines were incubated in RPMI-1640 medium with 10% fetal bovine serum at 37 °C. The cells were incubated with different concentration of the compound (0.39 – 100 μM) for 24 h. The reported methodology of MTT colorimetric assay was then applied [57].

4.2.2. Antiangiogenic activity preliminary study

The enzyme inhibition assay of compound **4f** against VEGFR2, PDGFRα and PDGFRß was performed at the Egyptian company for the production of vaccines, sera, and drugs VACSERA, Giza, EGYPT. This was carried out using BPS Bioscience® VEGFR2 (KDR) Kinase and PDGFRα (D842I) Assay Kits with PDGFRα (D842I), GST-Tag (BPS Bioscience) or Recombinant Human PDGFRß, GST-tagged (Creative BioMart) according to the manufacturer's manual. The assay was carried at concentrations 10–10000 nM for VEGFR2 and PDGFRα, and at 1–1000 nM for PDGFRß using 20 μL of the diluted enzyme (1 ng/μL). (For more information, see **Appendix A**)

4.2.3. Cell cycle analysis and apoptosis study

Cell cycle analysis of compound **4f** was achieved using propidium iodide (PI) flow cytomertric analysis according to the reported procedure [106,107]. An apoptotic study using the Annexin V-FITC Apoptosis Detection Kit (K101-25, BioVision®, Mountain View, Canada), was performed on compound **4f** at the Egyptian company for the production of vaccines, sera, and drugs VACSERA, Giza, EGYPT. The assay was measured at its IC_{50} concentration value on both CAKI-1 and UO-31 renal cells after 24 h in three successive steps; according to the manufacturer's instructions.

4.2.4. In vitro CDK inhibitory activity

IC_{50} values of compound **4f** were estimated using enzyme-linked immunosorbent assay kits for CDK1a (Cloud clone prob.®), CDK1b (Cell signaling Technology®) and CDK2a (Bioscience.com) at the Egyptian company for the production of vaccines, sera, and drugs VACSERA, Giza, EGYPT following the kits suppliers protocols. The assay was carried at concentrations 10–10000 nM for CDK1b and CDK2a using enzyme concentration (~5 ng/μL) and at 1–1000 nM for CDK1a using enzyme concentration (~3.5 ng/μL). (For more information, see **Appendix A**)

4.3. In silico studies

4.3.1. Drug likeness profile

The pharmacokinetic and physicochemical data of compound **4f** was calculated using the free online web tool swissADME (http://swissadme.ch/index.php#undefined) [108].

4.3.2. Docking study

Molecular docking studies were performed using the Molecular Operating Environment (MOE, 10.2008) software. Minimization was done with MOE until an RMSD gradient of 0.05 $kcal \cdot mol^{-1}Å^{-1}$ with MMFF94x forcefield. Partial charges were automatically calculated. The X-ray crystallographic structure of PDGFRα, co-crystallized with WQ-C-159 was retrieved from the Protein Data Bank, https://www.rcsb.org/, (PDB code: 5GRN) [109]. The enzyme was prepared by removing the water molecules. Protonation of the enzyme was done using protonate 3D protocol in MOE with the default parameters. Docking protocol was carried out using Triangle Matcher placement method while London dG scoring function were used for the docking protocol and the produced poses were refined using forcefield. Redocking of the native ligand into the active site was carried out with the purpose of docking setup validation. After then, the validated setup was used to predict the possible binding pose of compound **4f** to be compared to that of sunitinib as reference compound and so its affinity to the target enzyme.

4.4. Pharmacokinetic study

Pharmacokinetic properties of compound **4f** were determined following i.v. and p.o. administration in male Sprague-Dawley rats

(250–300 g) obtained from the Laboratory Animal Center, Faculty of Pharmacy, Cairo University. Approval of all experimental procedures was obtained from the Research Ethics Committee for experimental and clinical studies at Faculty of Pharmacy, Cairo University. The animals were placed in cages with free access to food and water. Compound **4f** was dissolved with the aid of 5% tween 80 in normal saline. Animals were randomly divided into two groups (n = 4). The first group was orally dosed with 15 mg/kg of compound **4f** by gastric gavage. The second group was given a dose of 5 mg/kg by gastric gavage injection into the tail vein. After then, blood samples (200 μL) were withdrawn from the orbital venous plexus at the following time intervals: 30 min and 1, 2, 3, 4, 5, 6, 8 and 24 h (p.o.); 5, 20, 40 min and 1, 2, 4, 6, 8 and 24 h (i.v.). Whole blood samples were collected in heparinized tubes and the plasma was immediately centrifuged (4000 rpm, 10 min, 4 °C) and then stored at − 20 °C until analysis. For preparation of the calibration curve, compound **4f** was dissolved in acetonitrile at a concentration of 0.5 mg/mL (Working solution), and then seven calibration standards ranging from 50 to 9000 ng/mL of **4f** were prepared by adding 10 μL of serial dilutions from the working solution to 90 μL of drug free rat plasma. The calibration standards and the plasma samples were extracted by protein precipitation using acetonitrile. The concentrations of compound **4f** in the extracted standards and plasma samples were quantified by LC-UV with a reversed-phase column (Waters Spherisorb ODS column (150 × 4.6 mm, 5 μm) (column temperature = 45 ± 2 °C) and acetonitrile: 0.1% triethylamine (50:50, v/v) as the mobile phase. The flow rate was maintained at 1 mL/min and UV detection at 341 nm. The pharmacokinetics parameters were calculated using WinNonlin Software 7.0 [110,111].

4.5. IC_{50} calculations and statistical analysis

All IC50 calculations were carried out using Quest Graph™ IC50 Calculator, which uses a four-parameter logistic regression model [112]. The results presented herein are expressed as mean ± SD. Statistical significance of the IC_{50} values was checked using GraphPad Prism 7.00 software using the Student's *t*-test at $P < 0.05$.

Funding:

This research did not receive any specific grant from funding agencies in the public, commercial, or not-for-profit sectors.

Declaration of Competing Interest

The authors declare that they have no known competing financial interests or personal relationships that could have appeared to influence the work reported in this paper.

Appendix A. Supplementary material

Supplementary data to this article can be found online at https://doi.org/10.1016/j.bioorg.2021.104985.

References:

[1] American Cancer Society "Cancer Facts and Figures", (2021) 1–72.
[2] T. Alonso-Gordoa, M.L. García-Bermejo, E. Grande, P. Garrido, A. Carrato, J. Molina-Cerrillo, Targeting Tyrosine kinases in Renal Cell Carcinoma: "New Bullets against Old Guys, Int. J. Mol. Sci. 20 (2019) 1–24.
[3] V.E. Reuter, S.K. Tickoo, Differential diagnosis of renal tumours with clear cell histology, Pathology 42 (2010) 374–783.
[4] S. Nabi, E.R. Kessler, B. Bernard, T.W. Flaig, E.T. Lam, Renal cell carcinoma: a review of biology and pathophysiology, F1000, Research 7 (2018) 307.
[5] L. Mologni, Development of RET kinase inhibitors for targeted cancer therapy, Curr. Med. Chem. 18 (2011) 162–175.
[6] M. Song, Recent developments in small molecule therapies for renal cell carcinoma, Eur. J. Med. Chem. 142 (2017) 383–392.
[7] V.R. Adams, M. Leggas, Sunitinib malate for the treatment of metastatic renal cell carcinoma and gastrointestinal stromal tumors, Clin. Ther. 29 (2007) 1338–1353.
[8] D.B. Mendel, A.D. Laird, X. Xin, S.G. Louie, J.G. Christensen, G. Li, R.E. Schreck, T.J. Abrams, T.J. Ngai, L.B. Lee, L.J. Murray, J. Carver, E. Chan, K.G. Moss, J. O. Haznedar, J. Sukbuntherng, R.A. Blake, L. Sun, C. Tang, T. Miller, S. Shirazian, G. McMahon, J.M. Cherrington, *In vivo* antitumor activity of SU11248, a novel tyrosine kinase inhibitor targeting vascular endothelial growth factor and platelet-derived growth factor receptors: determination of a pharmacokinetic/pharmacodynamic relationship, Clin. Cancer Res. 9 (2003) 327–337.
[9] R.J. Motzer, T.E. Hutson, P. Tomczak, M.D. Michaelson, R.M. Bukowski, O. Rixe, S. Oudard, S. Negrier, C. Szczylik, S.T. Kim, I. Chen, P.W. Bycott, C.M. Baum, R. A. Figlin, Sunitinib versus interferon alfa in metastatic renal-cell carcinoma, N. Engl. J. Med. 356 (2007) 115–124.
[10] M. Rizzo, C. Porta, Sunitinib in the treatment of renal cell carcinoma: an update on recent evidence, Therap. adv. urol. 9 (2017) 195–207.
[11] B.I. Rini, T.E. Hutson, R.A. Figlin, M.J. Lechuga, O. Valota, L. Serfass, B. Rosbrook, R.J. Motzer, Sunitinib in Patients With Metastatic Renal Cell Carcinoma: Clinical Outcome According to International Metastatic Renal Cell Carcinoma Database Consortium Risk Group, Clin. Genitourin. Cancer 16 (2018) 298–304.
[12] S. Giuliano, Y. Cormerais, M. Dufies, R. Grepin, P. Colosetti, A. Belaid, J. Parola, A. Martin, S. Lacas-Gervais, N.M. Mazure, R. Benhida, P. Auberger, B. Mograbi, G. Pages, Resistance to sunitinib in renal clear cell carcinoma results from sequestration in lysosomes and inhibition of the autophagic flux, Autophagy 11 (2015) 1891–1904.
[13] L. Zhou, X.D. Liu, M. Sun, X. Zhang, P. German, S. Bai, Z. Ding, N. Tannir, C. G. Wood, S.F. Matin, J.A. Karam, P. Tamboli, K. Sircar, P. Rao, E.B. Rankin, D. A. Laird, A.G. Hoang, C.L. Walker, A.J. Giaccia, E. Jonasch, Targeting MET and AXL overcomes resistance to sunitinib therapy in renal cell carcinoma, Oncogene 35 (2016) 2687–2897.
[14] P.J. Siska, K.E. Beckermann, W.K. Rathmell, S.M. Haake, Strategies to overcome therapeutic resistance in renal cell carcinoma, Urol. Oncol. 35 (2017) 102–110.
[15] H. Butz, Q. Ding, R. Nofech-Mozes, Z. Lichner, H. Ni, G.M. Yousef, Elucidating mechanisms of sunitinib resistance in renal cancer: an integrated pathological-molecular analysis, Oncotarget 9 (2017) 4661–4674.
[16] N. Yamaguchy, M. Osaki, K. Onuma, T. Yumioka, H. Iwamoto, T. Sejima, H. Kugoh, A. Takenaka, F. Okada, Identification of MicroRNAs Involved in Resistance to Sunitinib in Renal Cell Carcinoma Cells, Anticancer Res. 37 (2017) 2985–2992.
[17] S.P. Robinson, J.K.R. Boult, N.S. Vasudev, A.R. Reynolds, Monitoring the Vascular Response and Resistance to Sunitinib in Renal Cell Carcinoma In Vivo with Susceptibility Contrast MRI, Cancer Res. 77 (2017) 4127–4134.
[18] P. Makhov, S. Joshi, P. Ghatalia, A. Kutikov, R.G. Uzzo, V.M. Kolenko, Resistance to Systemic Therapies in Clear Cell Renal Cell Carcinoma: Mechanisms and Management Strategies, Mol. Cancer Ther. 17 (2018) 1355–1364.
[19] A. Sánchez-Gastaldo, E. Kempf, A. González del Alba, I. Duran, Systemic treatment of renal cell cancer: A comprehensive review, Cancer Treat. Rev. 60 (2017) 77–89.
[20] X. Guo, R. Li, Q. Bai, S. Jiang, H. Wang, TFE3-PD-L1 axis is pivotal for sunitinib resistance in clear cell renal cell carcinoma, J. cell. mol. med. 24 (2020) 14441–14452.
[21] M.M. Mita, E.K. Rowinsky, L. Forero, S.G. Eckhart, E. Izbicka, G.R. Weiss, M. Beeram, A.C. Mita, J.S. de Bono, A.W. Tolcher, L.A. Hammond, P. Simmons, K. Berg, C. Takimoto, A. Patnaik, A phase II, pharmacokinetic, and biologic study of semaxanib and thalidomide in patients with metastatic melanoma, Cancer Chemother. Pharmacol. 59 (2007) 165–174.
[22] J.J. Haddad, The immunopharmacologic potential of Semaxanib and new generation directed therapeutic drugs: Receptor tyrosine kinase regulation with anti-tumorigenensis/angiogenesis properties, Saudi pharm. j. 20 (2012) 103–123.
[23] K. Fukunaga, S. Yokoe, S. Kawashima, Y. Uchida, H. Nakagawa, Y. Nakano, Nintedanib prevented fibrosis progression and lung cancer growth in idiopathic pulmonary fibrosis, Respir. Case Rep. 6 (2018) 1–3.
[24] A.D. Laird, P. Vajkoczy, L.K. Shawver, A. Thurnher, C. Liang, M. Mohammadi, J. Schlessinger, A. Ullrich, S.R. Hubbard, R.A. Blake, T.A. Fong, L.M. Strawn, L. Sun, C. Tang, R. Hawtin, F. Tang, N. Shenoy, K.P. Hirth, G. McMahon, Cherrington, SU6668 is a potent antiangiogenic and antitumor agent that induces regression of established tumors, Cancer Res. 60 (2000) 4152–4160.
[25] G. Cerchiaro, A.M.d.C. Ferreira, Oxindoles and copper complexes with oxindole-derivatives as potential pharmacological agents, J. Braz. Chem. Soc. 17 (2006) 1473–1485.
[26] M. Kidwai, A. Jahan, N.K. Mishra, Isatins: A Diversity Orientated Biological Profile, Med. Chem. 4 (2014) 451–468.
[27] A. Cane, M.-C. Tournaire, D. Barritault, M. Crumeyrolle-Arias, The Endogenous Oxindoles 5-Hydroxyoxindole and Isatin Are Antiproliferative and Proapoptotic, Biochem. Biophys. Res. Comm. 276 (2000) 379–384.
[28] D. Havrylyuk, N. Kovach, B. Zimenkovsky, O. Vasylenko, R. Lesyk, Synthesis and anticancer activity of isatin-based pyrazolines and thiazolidines conjugates, Arch. Pharm. 344 (2011) 514–522.
[29] K.L. Vine, L. Matesic, J.M. Locke, M. Ranson, D. Skropeta, Cytotoxic and anticancer activities of isatin and its derivatives: a comprehensive review from 2000–2008, Anticancer Agents Med. Chem. 9 (2009) 397–414.
[30] G. Krishnegowda, A.S. Prakasha Gowda, H.R. Tagaram, K.F. Carroll, R.B. Irby, A. K. Sharma, S. Amin, Synthesis and biological evaluation of a novel class of isatin analogs as dual inhibitors of tubulin polymerization and Akt pathway, Bioorg. Med. Chem. 19 (2011) 6006–6014.
[31] K.L. Vine, L. Belfiore, L. Jones, J.M. Locke, S. Wade, E. Minaei, M. Ranson, N-alkylated isatins evade P-gp mediated efflux and retain potency in MDR cancer cell lines, Heliyon, 2 (2016) 1-23.
[32] Sonam Varun, R. Kakkar, Isatin and its derivatives: a survey of recent syntheses, reactions, and applications, MedChemComm. 10 (2019) 351–368.

[33] Y. Chang, Y. Yuan, Q. Zhang, Y. Rong, Y. Yang, M. Chi, Z. Liu, Y. Zhang, P. Yu, Y. Teng, Effects of an isatin derivative on tumor cell migration and angiogenesis, RSC Adv. 10 (2020) 1191–1197.
[34] N.R. Penthala, T.R. Yerramreddy, N.R. Madadi, P.A. Crooks, Synthesis and in vitro evaluation of N-alkyl-3-hydroxy-3-(2-imino-3-methyl-5-oxoimidazolidin-4-yl)indolin-2-one analogs as potential anticancer agents, Bioorg. Med. Chem. Lett. 20 (2010) 4468–4471.
[35] Ö. Güzel-Akdemir, A. Akdemir, N. Karalı, C.T. Supuran, Discovery of novel isatin-based sulfonamides with potent and selective inhibition of the tumor-associated carbonic anhydrase isoforms IX and XII, Org. Biomolec. Chem. 13 (2015) 6493–6499.
[36] W.M. Eldehna, A. Altoukhy, H. Mahrous, H.A. Abdel-Aziz, Design, synthesis and QSAR study of certain isatin-pyridine hybrids as potential anti-proliferative agents, Eur. J. Med. Chem. 90 (2015) 684–694.
[37] D. Havrylyuk, B. Zimenkovsky, O. Vasylenko, A. Gzella, R. Lesyk, Synthesis of New 4-Thiazolidinone-, Pyrazoline-, and Isatin-Based Conjugates with Promising Antitumor Activity, Med. Chem. 55 (2012) 8630–8641.
[38] S. Wang, Y. Zhao, G. Zhang, Y. Lv, N. Zhang, P. Gong, Design, synthesis and biological evaluation of novel 4-thiazolidinones containing indolin-2-one moiety as potential antitumor agent, Eur. J. Med. Chem. 46 (2011) 3509–3518.
[39] P.K. Ramshid, S. Jagadeeshan, A. Krishnan, M. Mathew, S.A. Nair, M.R. Pillai, Synthesis and in vitro evaluation of some isatin-thiazolidinone hybrid analogues as anti-proliferative agents, Med. Chem. 6 (2010) 306–312.
[40] D. Kaminskyy, D. Khyluk, O. Vasylenko, L. Zaprutko, R. Lesyk, A facile synthesis and anticancer activity evaluation of spiro[thiazolidinone-isatin] conjugates, Sci. pharm. 79 (2011) 763–777.
[41] A. Benmohammed, O. Khoumeri, A. Djafri, T. Terme, P. Vanelle, Synthesis of novel highly functionalized 4-thiazolidinone derivatives from 4-phenyl-3-thiosemicarbazones, Molecules (Basel, Switzerland) 19 (2014) 3068–3083.
[42] S. Sardari, S. Feizi, A.H. Rezayan, P. Azerang, S.M. Shahcheragh, G. Ghavami, A. Habibi, Synthesis and Biological Evaluation of Thiosemicarbazide Derivatives Endowed with High Activity toward Mycobacterium Bovis, Iran J. Pharm. Res. 16 (2017) 1128–1140.
[43] M.W. Beukers, M.J. Wanner, J.K. Von Frijtag Drabbe, E.C. Kunzel, I.J.A. P. Klaasse, G.J. Koomen, N6-cyclopentyl-2-(3-phenylaminocarbonyltriazene-1-yl) adenosine (TCPA), a very selective agonist with high affinity for the human adenosine A1 receptor, J. Med. Chem. 46 (2003) 1492–1503.
[44] B.X. Hu, Z.L. Shen, J. Lu, X.Q. Hu, W.M. Mo, N. Sun, D. Xu, Synthesis and Characterization of New Thiazolidin-4-one Derivatives, Phosphorus Sulfur Silicon Relat. Elem. 184 (2009) 523–535.
[45] A.A. Khan, N. Siddiqui, M.J. Akhtar, Z. Ali, M.S. Yar, Design, Synthesis, and Biological Evaluation of 6-(2-Amino-substituted phenyl)-4-(substituted phenyl)-1,2,4-triazine-3,5(2H,4H)-dione Derivatives as Anticonvulsant Agents, Arch. Pharm. 349 (2016) 277–292.
[46] L.F. Audrieth, The preparation of semicarbazide, J. Am. Chem. Soc. 52 (1930) 1250–1251.
[47] H. Pervez, Z.H. Chohan, M. Ramzan, F.-U.-H. Nasim, K.M. Khan, Synthesis and biological evaluation of some new N4-substituted isatin-3-thiosemicarbazones, J. Enz. Inh. Med. Chem. 24 (2009) 437–446.
[48] M.D. Hall, N.K. Salam, J.L. Hellawell, H.M. Fales, C.B. Kensler, J.A. Ludwig, G. Szakacs, D.E. Hibbs, M.M. Gottesman, Synthesis, activity, and pharmacophore development for isatin-beta-thiosemicarbazones with selective activity toward multidrug-resistant cells, J. Med. Chem. 52 (2009) 3191–3204.
[49] A. Qasem Ali, N.E. Eltayeb, S.G. Teoh, A. Salhin, H.K. Fun, (Z)-2-(2-Oxoindolin-3-yl-idene)-N-phenylhydrazinecarbothio-amide, Acta Crystallogr, Sect. E.-Struct Rep. Online 68 (2012) 962–963.
[50] A.Q. Ali, S.G. Teoh, A. Salhin, N.E. Eltayeb, M.B. Khadeer Ahamed, A.M. Abdul Majid, Synthesis of isatin thiosemicarbazones derivatives: in vitro anti-cancer, DNA binding and cleavage activities, Spectrochim. Acta A Mol. Biomol. Spectrosc. 125 (2014) 440–448.
[51] G. Pelosi, C. Pelizzi, M. Belicchi Ferrari, M.C. Rodriguez-Arguelles, C. Vieito, J. Sanmartin, Isatin 3-semicarbazone and 1-methylisatin 3-semicarbazone, Acta Crystallogr. C 61 (2005) 589–592.
[52] M. Cigan, K. Jakusov, J. Donovalov, V. Szocs, A. Gaplovsk, Isatin N-phenylsemicarbazone: effect of substituents and concentration on anion sensing selectivity and sensitivity, RSC Adv. 5 (2014) 54072–54079.
[53] F.A. Ragab, N.A. El-Sayed, A.A. Eissa, A.M. El Kerdawy, Synthesis and anticonvulsant activity of certain substituted furochromone, benzofuran and flavone derivatives, Chem. Pharm. Bull. 58 (2010) 1148–1156.
[54] A.S. Salman, N.A. Mahmoud, M.A. Mohamed, A. Abdel-aziem, D.M. Elsisi, Synthesis, Characterization and in vitro Cytotoxic Evaluation of Some Novel Heterocyclic Compounds Bearing Indole Ring, Am. J. Org. Chem. 6 (2016) 39–53.
[55] N. Hussain, A. Joshi, C. Sharma, G. Talesara, A Convenient Synthesis of Some New Indole Containing Thiazolidinone, Thiohydantoin, Triazine and its Derivatives with Ethoxyphthalimide Moiety, Asi. J. Chem. 24 (2012) 5917–5921.
[56] E.A. Mohamed, M.M. Ismail, Y. Gabr, M. Abass, Synthesis of Some Multiazaheterocycles as Substituents to Quinolone Moiety of Specific Biological Activity, Chem. Papers 48 (1994) 285–292.
[57] J.M. Edmondson, L.S. Armstrong, A.O. Martinez, A rapid and simple MTT-based spectrophotometric assay for determining drug sensitivity in monolayer cultures, J. Tissue Cult. Methods 11 (1988) 15–17.
[58] M. Greenblatt, P. Shubi, Tumor angiogenesis: transfilter diffusion studies in the hamster by the transparent chamber technique, J. Natl. Cancer Inst. 41 (1968) 111–124.
[59] Y. Cao, J. Arbiser, R.J. D'Amato, P.A. D'Amore, D.E. Ingber, R. Kerbel, M. Klagsbrun, S. Lim, M.A. Moses, B. Zetter, H. Dvorak, R. Langer, Forty-Year Journey of Angiogenesis Translational Research, Sci. Transl. Med. 3 (2011) 1–8.
[60] R.H. Adams, K. Alitalo, Molecular regulation of angiogenesis and lymphangiogenesis, Nat. Rev. Mol. Cell Biol. 8 (2007) 464–478.
[61] D. Hanahan, G. Christofori, P. Naik, J. Arbeit, Transgenic mouse models of tumour angiogenesis: the angiogenic switch, its molecular controls, and prospects for preclinical therapeutic models, Eur. J. Cancer 32 (1996) 2386–2393.
[62] M. Bianconi, L. Faloppi, A. Lopez-Beltran, M. Scarpelli, M. Scartozzi, L. Cheng, R. Montironi, Clinical impact of tumoral angiogenesis on renal cell carcinoma management: where do we stand? Exp. Rev. Pre. Med. Drug Dev. 1 (2016) 229–231.
[63] R. Iacovelli, A. Palazzo, P. Trenta, S. Mezi, D. Pellegrino, G. Naso, E. Cortesi, Management of metastatic renal cell carcinoma progressed after sunitinib or another antiangiogenic treatment, Am. J. Clin. Oncol. 37 (2014) 611–615.
[64] D.Y. Heng, W. Xie, M.M. Regan, M.A. Warren, A.R. Golshayan, C. Sahi, B.J. Eigl, J.D. Ruether, T. Cheng, S. North, P. Venner, J.J. Knox, K.N. Chi, C. Kollmannsberger, D.F. McDermott, W.K. Oh, M.B. Atkins, R.M. Bukowski, B. I. Rini, T.K. Choueiri, Prognostic factors for overall survival in patients with metastatic renal cell carcinoma treated with vascular endothelial growth factor-targeted agents: results from a large, multicenter study, J. Clin. Oncol. 27 (2009) 5794–5799.
[65] X. Na, G. Wu, C.K. Ryan, S.R. Schoen, P.A. Di'Santagnese, E.M. Messing, Overproduction of vascular endothelial growth factor related to von Hippel-Lindau tumor suppressor gene mutations and hypoxia-inducible factor-1 alpha expression in renal cell carcinomas, J. Urol. 170 (2003) 588–592.
[66] Y. Lai, Z. Zhao, T. Zeng, X. Liang, D. Chen, X. Duan, G. Zeng, W. Wu, Crosstalk between VEGFR and other receptor tyrosine kinases for TKI therapy of metastatic renal cell carcinoma, Cancer Cell Int. 18 (2018) 1–9.
[67] J. Donovan, X. Shiwen, J. Norman, D. Abraham, Platelet-derived growth factor alpha and beta receptors have overlapping functional activities towards fibroblasts, Fibrogenesis Tissue Repair 6 (2013) 1–9.
[68] A.A. Cumpanas, A.M. Cimpean, O. Ferician, R.A. Ceausu, S. Sarb, V. Barbos, A. Dema, M. Raica, The Involvement of PDGF-B/PDGFRbeta Axis in the Resistance to Antiangiogenic and Antivascular Therapy in Renal Cancer, Anticancer Res. 36 (2016) 2291–2295.
[69] R. Roskoski Jr., Sunitinib: a VEGF and PDGF receptor protein kinase and angiogenesis inhibitor, Biochem. Biophys. Res. Commun. 356 (2007) 323–328.
[70] I. Sulzbacher, P. Birner, M. Träxler, M. Marberger, A. Haitel, Expression of Platelet-Derived Growth Factor-α Receptor Is Associated With Tumor Progression in Clear Cell Renal Cell Carcinoma, Am. J. Clin. Pathol. 120 (2003) 107–112.
[71] L.F. Qi, D. Sun, J.H. Zheng, J. Du, X. Yao, Detection and clinical significance of platelet derived growth factor-BB and microvessel density in clear cell renal cell carcinoma, Chin. J. Oncol. 35 (2013) 672–677.
[72] C.Y. Yu, C.L. Jerry Teng, P.S. Hung, C.C. Cheng, S.L. Hsu, G.Y. Hwang, Y. M. Tzeng, Ovatodiolide isolated from Anisomeles indica induces cell cycle G2/M arrest and apoptosis via a ROS-dependent ATM/ATR signaling pathways, Eur. J. Pharmacol. 819 (2018) 16–29.
[73] W.M. Eldehna, M.F. Abo-Ashour, H.S. Ibrahim, G.H. Al-Ansary, H.A. Ghabbour, M.M. Elaasser, H.Y.A. Ahmed, N.A. Safwat, Novel [(3-indolylmethylene) hydrazono]indolin-2-ones as apoptotic anti-proliferative agents: design, synthesis and in vitro biological evaluation, J. Enz. Inhib. Med. Chem. 33 (2018) 686–700.
[74] J.W. Harper, P.D. Adams, Cyclin-dependent kinases, Chem. Rev. 101 (2001) 2511–2526.
[75] M.K. Diril, C.K. Ratnacaram, V.C. Padmakumar, T. Du, M. Wasser, V. Coppola, L. Tessarollo, P. Kaldis, Cyclin-dependent kinase 1 (Cdk1) is essential for cell division and suppression of DNA re-replication but not for liver regeneration, Proc. Natl. Acad. Sci. U.S.A. 109 (2012) 3826–3831.
[76] N.R. Brown, S. Korolchuk, M.P. Martin, W.A. Stanley, R. Moukhametzianov, M.E. M. Noble, J.A. Endicott, CDK1 structures reveal conserved and unique features of the essential cell cycle CDK, Nat. Commun. 6 (2015) 1–12.
[77] I. Neganova, F. Vilella, S.P. Atkinson, M. Lloret, J.F. Passos, T. von Zglinicki, J. E. O'Connor, D. Burks, R. Jones, L. Armstrong, M. Lako, An important role for CDK2 in G1 to S checkpoint activation and DNA damage response in human embryonic stem cells, Stem Cells 29 (2011) 651–659.
[78] H. Waterbeemd, Modern Methods of Drug Discovery, Third ed., Birkhäuser Basel (2003).
[79] A. Daina, O. Michielin, V. Zoete, SwissADME: a free web tool to evaluate pharmacokinetics, drug-likeness and medicinal chemistry friendliness of small molecules, Sci Rep 7 (2017) 42717.
[80] http://www.swissadme.ch/index.php.
[81] J.H. Martin, E.J. Begg, M.A. Kennedy, R. Roberts, M.L. Barclay, Is cytochrome P450 2C9 genotype associated with NSAID gastric ulceration? Br. J. Clin. Pharm. 51 (2001) 627–630.
[82] P. Hallberg, J. Karlsson, L. Kurland, L. Lind, T. Kahan, K. Malmqvist, K.P. Ohman, F. Nyström, H. Melhus, The CYP2C9 genotype predicts the blood pressure response to irbesartan: results from the Swedish Irbesartan Left Ventricular Hypertrophy Investigation vs Atenolol (SILVHIA) trial, J. Hypertens 20 (2002) 2089–2093.
[83] J. Schmider, D.J. Greenblatt, L.L. von Moltke, D. Karsov, R.I. Shader, Inhibition of CYP2C9 by selective serotonin reuptake inhibitors in vitro: studies of phenytoin p-hydroxylation, Br. J. Clin. Pharmacol. 44 (1997) 495–498.
[84] G.J. Gross, J.R. Falck, E.R. Gross, M. Isbell, J. Moore, K. Nithipatikom, Cytochrome P450 and arachidonic acid metabolites: Role in myocardial ischemia/reperfusion injury revisited, Cardiovasc. Res. 68 (2005) 18–25.

[85] J. Mwinyi, I. Cavaco, R.S. Pedersen, A. Persson, S. Burkhardt, S. Mkrtchian, M. Ingelman-Sundberg, Regulation of CYP2C19 expression by estrogen receptor α: implications for estrogen-dependent inhibition of drug metabolism, Mol. Pharmacol. 78 (2010) 886–894.
[86] S.-F. Zhou, L.-P. Yang, Z.-W. Zhou, Y.-H. Liu, E. Chan, Insights into the substrate specificity, inhibitors, regulation, and polymorphisms and the clinical impact of human cytochrome P450 1A2, The AAPS j. 11 (2009) 481–494.
[87] Q. Zhang, Z. Zhong, B. Li, Z. Liao, P. Zhao, Z. Ye, X. He, H. Wang, W. Chen, J. Huang, Effects of different CYP2C19 genotypes on prognosis of patients complicated with atrial fibrillation taking clopidogrel after PCI, Exp. Ther. Med. 16 (2018) 3492–3496.
[88] C.A. Lipinski, F. Lombardo, B.W. Dominy, P.J. Feeney, Experimental and computational approaches to estimate solubility and permeability in drug discovery and development settings, Adv. Drug Deliv. Rev. 46 (2001) 3–26.
[89] A.K. Ghose, V.N. Viswanadhan, J.J. Wendoloski, A Knowledge-Based Approach in Designing Combinatorial or Medicinal Chemistry Libraries for Drug Discovery. 1. A Qualitative and Quantitative Characterization of Known Drug Databases, J. Comb. Chem. 1 (1999) 55–68.
[90] D.F. Veber, S.R. Johnson, H.Y. Cheng, B.R. Smith, K.W. Ward, K.D. Kopple, Molecular properties that influence the oral bioavailability of drug candidates, J. Med. Chem. 45 (2002) 2615–5623.
[91] W.J. Egan, K.M. Merz Jr., J.J. Baldwin, Prediction of drug absorption using multivariate statistics, J. Med. Chem. 43 (2000) 3867–3877.
[92] I. Muegge, S.L. Heald, D. Brittelli, Simple Selection Criteria for Drug-like Chemical Matter, J. Med. Chem. 44 (2001) 1841–1846.
[93] R. Brenk, A. Schipani, D. James, A. Krasowski, I.H. Gilbert, J. Frearson, P. G. Wyatt, Lessons learnt from assembling screening libraries for drug discovery for neglected diseases, ChemMedChem. 3 (2008) 435–544.
[94] J.B. Baell, G.A. Holloway, New Substructure Filters for Removal of Pan Assay Interference Compounds (PAINS) from Screening Libraries and for Their Exclusion in Bioassays, J. Med. Chem. 53 (2010) 2719–2740.
[95] C. Muhle-Goll, S. Hoffmann, S. Afonin, S.L. Grage, A.A. Polyansky, D. Windisch, M. Zeitler, J. Bürck, A.S. Ulrich, Hydrophobic matching controls the tilt and stability of the dimeric platelet-derived growth factor receptor (PDGFR) β transmembrane segment, J. Biol. Chem. 287 (2012) 26178–26186.
[96] A.H.-R. Shim, H. Liu, P.J. Focia, X. Chen, P.C. Lin, X. He, Structures of a platelet-derived growth factor/propeptide complex and a platelet-derived growth factor/receptor complex, PNAS USA 107 (2010) 11307–11312.
[97] M.P. Martin, R. Alam, S. Betzi, D.J. Ingles, J.Y. Zhu, E. Schonbrunn, A novel approach to the discovery of small-molecule ligands of CDK2, Chembiochem 13 (2012) 2128–2136.
[98] A. Trojani, C.B. Ripamonti, S. Penco, A. Beghini, G. Nadali, E. Di Bona, A. Viola, C. Castagnola, P. Colapietro, G. Grillo, L. Pezzetti, E. Ravelli, M.C. Patrosso, A. Marocchi, A. Cuneo, F. Ferrara, M. Lazzarino, G. Pizzolo, R. Cairoli, E. Morra, Molecular analysis of PDGFRA and PDGFRB genes by rapid single-strand conformation polymorphism (SSCP) in patients with core-binding factor leukaemias with KIT or FLT3 mutation, Anticancer Res. 28 (2008) 2745–2751.
[99] S. Pundir, M.J. Martin, C. O'Donovan, UniProt Tools, Curr. Protoc. Bioinformatics, 53 (2016) 1.29.21-21.29.15.
[100] T.U. Consortium, UniProt: the universal protein knowledgebase in 2021, Nucleic Acids Res. 49 (2020) D480–D489.
[101] R. Roskoski Jr., Classification of small molecule protein kinase inhibitors based upon the structures of their drug-enzyme complexes, Pharmacol. Res. 103 (2016) 26–48.
[102] R. Roskoski Jr., The role of small molecule Kit protein-tyrosine kinase inhibitors in the treatment of neoplastic disorders, Pharmacol. Res. 133 (2018) 35–52.
[103] A. Monks, D. Scudiero, P. Skehan, R. Shoemaker, K. Paull, D. Vistica, C. Hose, J. Langley, P. Cronise, A. Vaigro-Wolff, et al., Feasibility of a high-flux anticancer drug screen using a diverse panel of cultured human tumor cell lines, J. Natl. Cancer Inst. 83 (1991) 757–766.
[104] M.R. Boyd, K.D. Paull, Some practical considerations and applications of the national cancer institute in vitro anticancer drug discovery screen, Drug Dev. Res. 34 (1995) 91–109.
[105] E.A. Orellana, A.L. Kasinski, Sulforhodamine B (SRB) Assay in Cell Culture to Investigate Cell Proliferation, Bio. Protoc. 6 (2016) 1–9.
[106] P. Pozarowski, Z. Darzynkiewicz, Analysis of cell cycle by flow cytometry, Methods Mol. Biol. 281 (2004) 301–311.
[107] L.C. Crowley, A.P. Scott, B.J. Marfell, J.A. Boughaba, G. Chojnowski, N. J. Waterhouse, Measuring Cell Death by Propidium Iodide Uptake and Flow Cytometry, Cold Spring Harb. Protoc. 2016 (2016) 647–652.
[108] A. Daina, V. Zoete, A BOILED-Egg To Predict Gastrointestinal Absorption and Brain Penetration of Small Molecules, ChemMedChem. 11 (2016) 1117–1121.
[109] https://www.rcsb.org/structure/5GRN.
[110] B.A. Moussa, A.A. El-Zaher, M.K. El-Ashrey, M.A. Fouad, Synthesis and molecular docking of new roflumilast analogues as preferential-selective potent PDE-4B inhibitors with improved pharmacokinetic profile, Eur. J. Med. Chem. 148 (2018) 477–486.
[111] B.A. Moussa, A.A. El-Zaher, M.K. El-Ashrey, M.A. Fouad, Roflumilast analogs with improved metabolic stability, plasma protein binding, and pharmacokinetic profile, Drug Test. Anal. 11 (2019) 886–897.
[112] "Quest GraphTM IC50 Calculator." AAT Bioquest, Inc, 16 Jan. 2021, https://www.aatbio.com/tools/ic50-calculator.